Terthienyl and Poly-terthienyl Ligands as Redox-Switchable Hemilabile Ligands for Oxidation-State-Dependent Molecular Uptake and Release

Dana A. Weinberger,[†] Thomas B. Higgins,[†] Chad A. Mirkin,*[,†] Charlotte L. Stern,[†] Louise M. Liable-Sands,[‡] and Arnold L. Rheingold[‡]

Contribution from the Department of Chemistry, Northwestern University, 2145 Sheridan Road, Evanston, Illinois 60208, and Department of Chemistry and Biochemistry, University of Delaware, Newark, Delaware 19716

Received August 11, 2000

Abstract: Mononuclear, dinuclear, and polymeric Ru(II) complexes formed from terthienylalkylphosphino redox-switchable hemilabile ligands demonstrate that this class of ligand provides electrochemical control over the electronic properties, coordination environments, and reactivities of bound transition metals. Specifically, [CpRuCO(κ^2-3′-(2-diphenylphosphinoethyl)-5,5″-dimethyl-2,2′:5′,2″-terthiophene)][B(C_6H_3-3,5-(CF_3)$_2$)$_4$] (**4a**) exhibits a 3 orders of magnitude increase in binding affinity for acetonitrile upon terthienyl-based oxidation. FT-IR spectroelectrochemical experiments on **4a** indicate that terthienyl-based oxidation removes electron density from the metal center, equivalent to approximately 11−17% of the electronic change that occurs upon direct oxidation of Ru(II) to Ru(III) in analogous complexes. The spectroelectrochemical responses of **4a** were compared to those of dimeric and polymeric analogues of **4a**. The spectroelectrochemistry of the dimer is consistent with two sequential, one-electron ligand-based oxidations, compared to only one in **4a**. In contrast, the polymer exhibits spectroelectrochemical behavior similar to that of **4a**. The polymer spectroelectrochemistry shows changes in the metal center electronic properties between two different states, reflective of two discrete oxidation states of the polymeric ligand backbone. We propose that the polymer backbone does not allow one to vary the electronic properties of the metal center through a continuous range of oxidation states due to charge localization within the metalated films. In an effort to explore the molecular uptake and release properties of **4a** and its polymer analogue as a function of ligand oxidation state, the oxidation-state-dependent coordination chemistries of **4a** and **4a**$^+$ with a variety of substrates were examined.

Introduction

Redox-active ligands are beginning to be used extensively to control ligand binding properties and transition metal reactivity.[1] Thus far, studies pertaining to such ligands have focused almost exclusively upon metallocene-based structures susceptible to one-electron oxidation/reduction reactions (e.g., ferrocene and cobaltocene). However, redox-active ligands with multiple accessible oxidation states could provide greater control and tailorability over the metal centers to which they are bound.

Our research group and others have pursued a decade-long goal of preparing conducting polymer−metal complexes in an effort to evaluate their potential as high-surface-area, electrode-immobilized materials with redox properties that allow one to electrochemically "tune", or vary through a continuum of redox states, the electron density at bound transition metal centers.[2−4] It has been hypothesized that such an approach could lead to materials with electrochemically variable transition metal reactivity.[2−4] Previously, Wolf and Wrighton prepared poly-[5,5′-(2-thienyl)-2,2′-bithiazole] and subsequently functionalized the backbone of this conducting polymer with cationic Re carbonyl fragments.[4] Although only modest metal-centered changes were noted upon polymer ligand-based oxidation, this novel material provided important initial insight into the use of conducting polymer films as substitutionally inert modalities for electrochemically modulating the electronic nature of the bound Re centers. One limitation of the aforementioned system is that the organic polymer was functionalized with the metal fragments after polymerization, leading to a heterogeneous structure which was difficult to characterize. Furthermore, although several well-characterized conducting polymer/transition metal coordination complex precursors and polymers formed from them have been synthesized, there is no information regarding the utility of these polymers for electrochemically controlling the electronic properties and reactivity of the bound metal centers.[5−9]

* To whom correspondence should be addressed.
[†] Northwestern University.
[‡] University of Delaware.

(1) Allgeier, A. M.; Mirkin, C. A. *Angew. Chem., Int. Ed. Engl.* **1998**, *37*, 894−908.
(2) Higgins, T. B.; Mirkin, C. A. *Chem. Mater.* **1998**, *10*, 1589−1595.
(3) Higgins, T. B.; Mirkin, C. A. *Inorg. Chim. Acta* **1995**, *240*, 347−353.
(4) Wolf, M. O.; Wrighton, M. S. *Chem. Mater.* **1994**, *6*, 1526−1533.
(5) Reddinger, J. L.; Reynolds, J. R. *Chem. Mater.* **1998**, *10*, 3−5.
(6) Martin, K. F.; Hanks, T. W. *Organometallics* **1997**, *16*, 4857−4860.
(7) Martin, K.; Dotson, M.; Litterer, M.; Hanks, T. W.; Veas, C. *Synth. Met.* **1996**, *78*, 161−168.
(8) Zhu, S. S.; Carroll, P. J.; Swager, T. M. *J. Am. Chem. Soc.* **1996**, *118*, 8713−8714.
(9) Clot, O.; Wolf, M. O.; Yap, G. P. A.; Patrick, B. O. *J. Chem. Soc., Dalton Trans.* **2000**, *16*, 2729−2737.

10.1021/ja0030008 CCC: $20.00
Published on Web 02/21/2001

Scheme 1

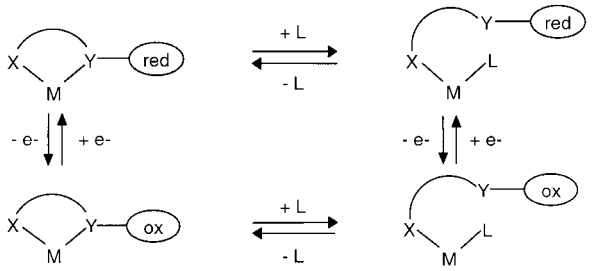

By extending the concept of redox-switchable hemilabile ligands (RHLs)[2,3,10−15] to conducting polymers, we have designed ligands in which a polymer backbone can be used to electrochemically modulate the electronic properties and coordination spheres of bound transition metals. With RHLs, one functional group on a bidentate ligand binds strongly to a chosen transition metal, and another functional group binds weakly, Scheme 1. The weakly bonding group also is in direct electronic communication with a pendant redox-active group. Upon oxidation and subsequent reduction of the pendant redox group, the strength of the interaction between the weakly bonding group and the metal center can be reversibly controlled. Significantly, the decrease in RHL binding constant for the metal center upon ligand-centered oxidation effectively increases the complex's binding affinity for substrates (L) in solution, Scheme 1. RHLs thereby provide an electrochemical means of controlling both the electronic and steric environments of metal centers. For this reason, it is thought that such complexes could be useful for electrochemically controllable catalytic or small-molecule uptake and release reactions (i.e., molecular separations).[1,16]

Herein, we report the synthesis, characterization, and reactivity of mononuclear, dinuclear, and polynuclear Ru(II) complexes formed from terthienyl-based RHLs. The design of these ligands takes into account several key considerations. First, such ligands are hemilabile when bound to Ru(II) via a substitutionally inert phosphine group and a relatively substitutionally labile thienyl moiety.[17,18] Second, the lower oxidation/reduction potentials for the ligand- compared to the metal-based redox reactions enable one to address ligand-based redox properties separate from metal-centered ones. Third, methyl-capped ligands allow for the controlled electrochemical study of mononuclear RHL−metal complexes, whereas hydrogen atoms in the terminal α-positions allow for the oxidative polymerization of the transition metal complexes formed from these ligands.[19−30] The direct polymerization of the metal-containing monomer avoids the post-polymerization functionalization of resultant polymers with the metal centers of interest, which inherently leads to questions regarding the degree and nature of functionalization.

Scheme 2

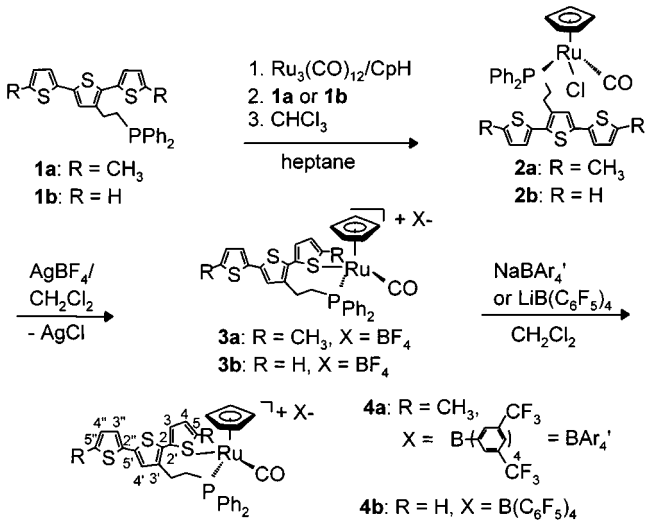

Results

Synthesis and Characterization of Terthienyl-Based Ligands, 1a and 1b. A methyl-capped terthienylalkylphosphine ligand, 3′-(2-diphenylphosphinoethyl)-5,5″-dimethyl-2,2′:5′,2″-terthiophene (**1a**), was synthesized[14] in order to prepare metal−ligand complexes suitable for solution electrochemical and spectroelectrochemical studies. Polymerizable ligand−metal complexes can be prepared from a hydrogen-atom-terminated analogue of **1a**, 3′-(2-diphenylphosphinoethyl)-2,2′:5′,2″-terthiophene (**1b**), which was synthesized by methods analogous to those used for the preparation of **1a**.[14] These ligands were fully characterized, and all data are consistent with their proposed structural formulations.

Synthesis and Characterization of a Ru(II)−Terthienyl Complex, 2a. Ligand **1a** was complexed to Ru(II) to form CpRuCOCl(3′-(2-diphenylphosphinoethyl)-5,5″-dimethyl-2,2′:5′,2″-terthiophene) (**2a**), Scheme 2. Complex **2a** was fully characterized in solution and in the solid state, and the solution spectroscopic data for this complex are consistent with its solid-state structure, which was determined by a single-crystal X-ray diffraction study (see Supporting Information). Moreover, the data are similar to those reported for isoelectronic, non-thienyl-group-containing complexes.[31] For example, the FT-IR CO stretching frequency at 1955 cm^{-1} for **2a** in CH_2Cl_2 compares

(10) Singewald, E. T.; Mirkin, C. A.; Stern, C. L. *Angew. Chem., Int. Ed. Engl.* **1995**, *34*, 1624−1627.
(11) Sassano, C. A.; Mirkin, C. A. *J. Am. Chem. Soc.* **1995**, *117*, 11379−11380.
(12) Slone, C. S.; Mirkin, C. A.; Yap, G. P. A.; Guzei, I. A.; Rheingold, A. L. *J. Am. Chem. Soc.* **1997**, *119*, 10743−10753.
(13) Allgeier, A. M.; Slone, C. S.; Mirkin, C. A.; Liable-Sands, L. M.; Yap, G. P. A.; Rheingold, A. L. *J. Am. Chem. Soc.* **1997**, *119*, 550−559.
(14) Weinberger, D. A.; Higgins, T. B.; Mirkin, C. A.; Liable-Sands, L. M.; Rheingold, A. L. *Angew. Chem., Int. Ed. Engl.* **1999**, *38*, 2565−2568.
(15) Allgeier, A. M.; Singewald, E. T.; Mirkin, C. A.; Stern, C. L. *Organometallics* **1994**, *13*, 2928−2930.
(16) Slone, C. S.; Weinberger, D. A.; Mirkin, C. A. In *The Transition Metal Coordination Chemistry of Hemilabile Ligands*; Karlin, K. D., Ed.; John Wiley & Sons: New York, 1999; Vol. 48, pp 233−350.
(17) Benson, J. W.; Angelici, R. J. *Organometallics* **1992**, *11*, 922−927.
(18) Benson, J. W.; Angelici, R. J. *Organometallics* **1993**, *12*, 680−687.
(19) Hill, M. G.; Mann, K. R.; Miller, L. L.; Penneau, J.-F. *J. Am. Chem. Soc.* **1992**, *114*, 2728−2730.
(20) Graf, D. D.; Campbell, J. P.; Miller, L. L.; Mann, K. R. *J. Am. Chem. Soc.* **1996**, *118*, 5480−5481.
(21) Engelmann, G.; Stösser, R.; Kossmehl, G.; Jugelt, W.; Welzel, H.-P. *J. Chem. Soc., Perkin Trans. 2* **1996**, 2015−2019.
(22) Tanaka, K.; Matsuura, Y.; Oshima, Y.; Yamabe, T.; Hotta, S. *Synth. Met.* **1994**, *66*, 295−298.
(23) Hill, M. G.; Penneau, J.-F.; Zinger, B.; Mann, K. R.; Miller, L. L. *Chem. Mater.* **1992**, *4*, 1106−1113.
(24) Kirste, B.; Tian, P.; Kossmehl, G.; Engelmann, G.; Jugelt, W. *Magn. Reson. Chem.* **1995**, *33*, 70−76.
(25) Zotti, G.; Schiavon, G.; Berlin, A.; Pagani, G. *Chem. Mater.* **1993**, *5*, 430−436.
(26) Diers, J. R.; DeArmond, M. K.; Guay, J.; Diaz, A.; Wu, R.; Schumm, J. S.; Tour, J. M. *Chem. Mater.* **1994**, *6*, 327−332.
(27) Guay, J.; Kasai, P.; Diaz, A.; Wu, R.; Tour, J. M.; Dao, L. H. *Chem. Mater.* **1992**, *4*, 1097−1105.
(28) Zotti, G.; Schiavon, G.; Berlin, A.; Pagani, G. *Chem. Mater.* **1993**, *5*, 620−624.
(29) Bäuerle, P.; Segelbacher, U.; Maier, A.; Mehring, M. *J. Am. Chem. Soc.* **1993**, *115*, 10217−10223.
(30) Bäuerle, P. *Adv. Mater.* **1992**, *4*, 102−107.
(31) Blackmore, T.; Bruce, M. I.; Stone, F. G. A. *J. Chem. Soc. (A)* **1971**, 2376−2382.

well with the ν_{CO} band at 1958 cm^{-1} reported for $CpRu(PPh_3)(CO)(Cl)$[31] in CS_2. The UV−vis spectrum of **2a** exhibits a $\pi-\pi^*$ transition with λ_{max} at 353 nm ($\epsilon = 3.6 \times 10^4$ $L\cdot mol^{-1}\cdot cm^{-1}$), which is very similar to the $\pi-\pi^*$ transition for ligand **1a** (358 nm, $\epsilon = 3.8 \times 10^4$ $L\cdot mol^{-1}\cdot cm^{-1}$). The $E_{1/2}$ value associated with ligand-centered radical cation formation in **2a** (510 mV vs FcH/FcH^+) is near the potential associated with oxidation and reduction of 5,5′-dimethylterthiophene (vide infra).

Synthesis and Characterization of Complexes with a Ru(II)−Terthienyl Interaction, 3a and 4a. Complex **2a** can be converted to a cationic complex in which one thienyl moiety is bound to the Ru(II) center, [CpRuCO(κ^2-3′-(2-diphenylphosphinoethyl)-5,5″-dimethyl-2,2′:5′,2″-terthiophene)][BF_4] (**3a**), by stirring **2a** in methylene chloride with $AgBF_4$ at room temperature for 1 h, Scheme 2. Chloride abstraction from **2a** to form **3a** is accompanied by a change in the CO stretching frequency from 1955 to 1993 cm^{-1}. This change is a consequence of decreased back-bonding between the CO ligand and the metal center in the cationic complex **3a** as compared to that in **2a**. Complex **3a** was isolated and characterized in solution, and all solution spectroscopic data are consistent with its proposed structural formulation.

Complex **3a**, dissolved in methylene chloride, exhibits long-term stability (over three months) at room temperature, as evidenced by ^1H NMR, $^{31}P\{^1H\}$ NMR, and FT-IR spectroscopies. However, ligand-centered oxidation of **3a** (effected in a spectroelectrochemical cell by setting the working electrode potential to 800 mV vs an Ag wire in 0.1 M *n*-Bu_4NPF_6 in CH_2Cl_2) results in immediate decomposition of **3a**. The nature of this decomposition is unclear, but the decomposition does not occur in a solution of **3a** and 0.1 M *n*-Bu_4NPF_6 in CH_2Cl_2 in the absence of applied potential. The decomposition product exhibits an FT-IR ν_{CO} band at 1955 cm^{-1}, and although the decomposition product was not fully characterized, the frequency of this ν_{CO} band indicates the formation of a neutral $CpRu(CO)(PR_3)X$ adduct.

To obtain an electrochemically stable version of **3a**, an alternative high-oxidation-potential, weakly coordinating counterion was sought. Therefore, **4a** was prepared from **3a** via counterion metathesis with Na[B(3,5-$(CF_3)_2C_6H_3)_4$][32] ($NaBAr_4'$). Complex **4a** was fully characterized in solution and in the solid state by a single-crystal X-ray diffraction study (see Supporting Information), and all data are consistent with its proposed structural formulation. For example, the FT-IR ν_{CO} stretching frequency of **4a** at 1996 cm^{-1} is identical to the frequency reported for an isoelectronic and isostructural complex, [Cp(CO)(PPh_3)Ru(2,5-Me_2thiophene)]BF_4.[17] In the UV−vis spectrum of **4a**, the $\pi-\pi^*$ transition has a λ_{max} at 352 nm with a shoulder at 420 nm ($\epsilon = 2.7 \times 10^4$ $L\cdot mol^{-1}\cdot cm^{-1}$). Although this shoulder is not present in **2a**, the λ_{max} values for **2a** and **4a** are very similar, suggesting that the extent of conjugation does not change significantly upon oligothienyl binding to the metal center. Additionally, the ^1H NMR spectrum of **4a** exhibits the expected five thienyl resonances, with one set of ring resonances shifted downfield when compared with analogous resonances for the complex formed when CH_3CN displaces the thienyl group from the Ru center of **4a** (**5a**, vide infra). Specifically, one doublet at δ 7.09, which can be assigned to either H-3 or H-3″ on the basis of a characteristic terthienyl coupling constant ($J_{3-4} = 3.6$ Hz), and one doublet of doublets at δ 6.95 in **4a**, which can be assigned to either H-4 or H-4″ on the basis of coupling constants ($J_{3-4} = 3.6$ Hz, $J_{4-Me} = 1.6$ Hz),[33,34] are shifted downfield compared to the analogous resonances for **5a** (δ 6.72, 6.68, respectively). These changes strongly indicate that the shifted resonances are associated with the Ru-bound thienyl ring, and therefore, we assign the resonances at δ 7.09 and 6.72 to H-3 and δ 6.95 and 6.68 to H-4 in **4a** and **5a**, respectively. These data are consistent with the single-crystal X-ray diffraction study of **4a**,[14] in which the terminal ring closest to the methylene substituent is the metal-bound moiety (see Supporting Information). If the thienyl ring were bound through one of the double bonds, the proton resonances associated with the coordinated carbon atoms would be expected to shift much farther upfield to δ 3.0−3.5, as in complexes with η^2-thiophene[35] or η^2-ethylene (**12**, vide infra) moieties.

Variable-temperature $^{31}P\{^1H\}$ NMR spectroscopy studies provide further evidence for the η^1 binding of the S atom in the solution structure of **4a**. These studies show that at room temperature, the phosphorus resonance for **4a** (δ 33.1) is due to the signal averaging of two different resonances and, therefore, two different forms of the complex which undergo fast interconversion at room temperature on the NMR time scale. A $^{31}P\{^1H\}$ NMR spectrum of **4a** at −77 °C shows two unequally populated resonances (δ 47.0, 29.4; ratio 1:21) that have been assigned to two different diastereomers which interconvert by pyramidal inversion at the bound sulfur. This type of process has been observed with analogous thiophene complexes of Fe and Ru.[17,18,36,37] The coalescence temperature for this process was not determined due to the low signal intensity of the downfield resonance but was determined for the analogous process in **4b** (vide infra).

Synthesis and Characterization of a Polymerizable Ru(II)−Terthienyl Complex, 2b. A Ru(II) complex of **1b**, CpRuCOCl(3′-(2-diphenylphosphinoethyl)-2,2′:5′,2″-terthiophene) (**2b**), was prepared via a method analogous to the one used for preparing **2a**, Scheme 2. Complex **2b** was characterized in solution, and the solution spectroscopic data for this complex are consistent with its proposed formulation and are similar to those reported for **2a** (see Supporting Information).

Synthesis and Characterization of Polymerizable Complexes with Ru(II)−Terthienyl Interactions, 3b and 4b. Chloride abstraction from **2b** with $AgBF_4$ yields **3b**, which has been isolated and characterized in solution, Scheme 2. Counterion metathesis of **3b** with $LiB(C_6F_5)_4\cdot Et_2O$ yields **4b**, a cationic complex with one thienyl group bound to the metal center. Complex **4b** was fully characterized in solution and in the solid state, and its solution spectroscopic data are consistent with its proposed structural formulation. The UV−vis spectrum of **4b** exhibits a $\pi-\pi^*$ transition with a λ_{max} at 340 nm and a shoulder at 420 nm ($\epsilon = 1.9 \times 10^4$ $L\cdot mol^{-1}\cdot cm^{-1}$). The λ_{max} is at a slightly higher energy than the analogous transition for **4a**. This difference is due to the greater electron-donating properties of the methyl groups in **4a** as compared to the hydrogen atoms in **4b**. The shoulders observed in the spectra of **4a** and **4b** are not observed in the spectra of **2a** and **2b**. Although the assignment of these shoulders has not been established conclusively, they are present only for those complexes in which the terthienyl moiety is bound directly to the metal, and similar

(32) Brookhart, M.; Grant, B.; Volpe, A. F. *Organometallics* **1992**, *11*, 3920−3922.

(33) Rossi, R.; Carpita, A.; Ciofalo, M.; Lippolis, V. *Tetrahedron* **1991**, *47*, 8443−8460.

(34) Mac Eachern, A.; Soucy, C.; Leitch, L. C.; Arnason, J. T.; Morand, P. *Tetrahedron* **1988**, *44*, 2403−2412.

(35) Cordone, R.; Harman, W. D.; Taube, H. *J. Am. Chem. Soc.* **1989**, *111*, 5969−5970.

(36) Draganjac, M.; Ruffing, C. J.; Rauchfuss, T. B. *Organometallics* **1985**, *4*, 1909−1911.

(37) Goodrich, J. D.; Nickias, P. N.; Selegue, J. P. *Inorg. Chem.* **1987**, *26*, 3424−3426.

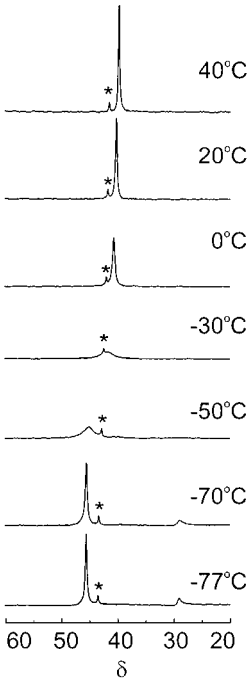

Figure 1. Variable-temperature $^{31}P\{^1H\}$ NMR spectra of **4b** in CD_2Cl_2. The asterisk indicates residual **2b** in solution.

shoulders have been noted in the spectra of polyalkylthiophenes to which $[CpFe(CO)_2]^+$ fragments are bound to the S atoms.[38] Complex **4b** was synthesized with a perfluorinated aryl borate counterion rather than the $[B(3,5\text{-}(CF_3)_2C_6H_3)_4]$ counterion used for **4a**, because the perfluorinated aryl borate yields higher quality polymers than does the counterion in **4a** (vide infra).

In the variable-temperature $^{31}P\{^1H\}$ NMR spectroscopy studies of **4b** in CD_2Cl_2, a single resonance at δ 40.2 is observed at room temperature, whereas at −77 °C resonances are observed at δ 45.2 and 28.8 with a signal intensity ratio of 28:1, respectively, Figure 1. Similar to the assignment for **4a**, these resonances were assigned to two different diastereomers which interconvert by pyramidal inversion at the bound sulfur. The two different free energies of activation ($\Delta G^{\ddagger}$), calculated[39] for the interconversion of the two unequally populated diastereomers at coalescence (206 K) in CD_2Cl_2, are 34.9 and 40.6 kJ/mol. By comparison, pyramidal sulfur inversions of substituted thiophenes bound in an η^1 fashion to Ru[17,18,36] and Fe[37] centers have been reported with $\Delta G^{\ddagger}$ values ranging from 39 to 43 kJ/mol. The intensities and chemical shifts of the peaks in the variable-temperature $^{31}P\{^1H\}$ NMR spectra of **4a** and **4b** suggest that the preferred diastereomeric configuration for **4b** in solution is opposite to the one preferred by **4a**.

Solid-State Structure of 4b. Crystals of **4b** suitable for single-crystal X-ray diffraction studies were grown by slow diffusion of pentane into a methylene chloride solution of **4b**, Figure 2 (see Supporting Information). Despite several attempts to recrystallize **4b**, the best crystals obtained were very weak and diffusely diffracting ($I/\sigma = 3.32$). Nevertheless, a single-crystal X-ray diffraction study of **4b** (BAr_4' counterion) provides connectivity data. It shows that the metal center has a tetrahedral coordination environment and that the κ^2 ligand binds through the phosphino moiety and the terminal thienyl ring closest to the methylene substituent (ring 1) in η^1 fashion. The thienyl

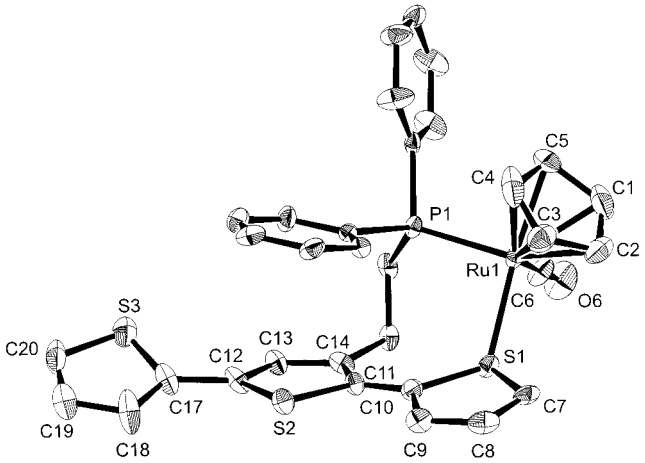

Figure 2. ORTEP diagram of **4b**. The $[B(3,5\text{-}(CF_3)_2C_6H_3)_4]$ counterion and hydrogen atoms are omitted for clarity, and thermal ellipsoids are drawn at 30% probability.

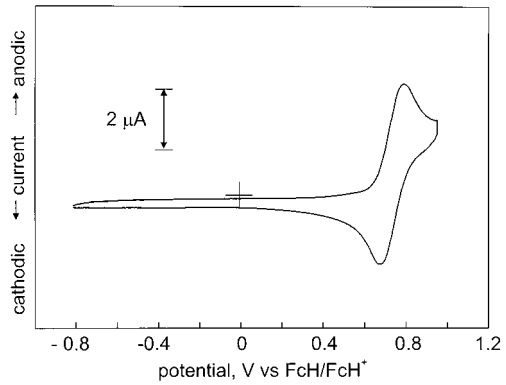

Figure 3. Cyclic voltammogram of **4a** in CH_2Cl_2/0.1 M *n*-Bu_4NPF_6 using an Au working electrode, Pt mesh counter electrode, and Ag wire quasi-reference electrode at a scan rate of 200 mV/s.

rings have an antiparallel arrangement, and the Ru−S bond length is 2.397(3) Å, similar to the Ru−S bond length in **4a** (2.3903(9) Å). The Ru-bound S atom has a pyramidal geometry, which is apparent from the Ru−S−midpoint (the midpoint of the vector between the carbon atoms α to the bound sulfur) angle, which is 127.8°, and a calculation of the sum of the angles formed by the S atom and its substituents (323.0°).[17,18] Just as low-temperature $^{31}P\{^1H\}$ NMR spectroscopy studies suggest that **4a** and **4b** have different preferred diasteromeric configurations in solution, the absolute diastereomeric configuration of **4b** in the solid state is Ru_SS_S/Ru_RS_R,[40] in contrast to that of **4a** (Ru_RS_S/Ru_SS_R).[14]

The inter-ring dihedral torsion angles in **4b** and other pertinent crystallographic data are summarized in Table 1. In **4b,** the S atom displacement is greatest for ring 1 and progressively diminishes for rings 2 and 3. In **2a**, the rings are generally comparable in planarity to those in **4a** and **4b**, as evidenced by S atom displacements and mean deviations of the thienyl atoms from the planes they comprise. In **4b**, the S−C bonds in the ring which is bound to Ru are longer than the S−C bonds in **2a**, and the average C−S bond length for each ring in **4b** decreases as the rings move farther away from the Ru atom. In contrast to this trend in C−S bond lengths, the C−S−C bond angles are not affected by binding of the S atom to Ru, similar to the trend observed for **4a** (see Supporting Information).

(38) Shaver, A.; Butler, I. S.; Gao, J. P. *Organometallics* **1989**, *8*, 2079−2080.

(39) Sandström, J. *Dynamic NMR Spectroscopy*; Academic Press: London, 1982.

(40) Ligand priority order: Ru (C_5H_5 > thiophene > phosphine > CO); S (Ru, C-thiophene, C−CH_3, lone pair). See: Stanley, K.; Baird, M. C. *J. Am. Chem. Soc.* **1975**, *97*, 6598.

Table 1. (a) Crystallographic Data and (b) Crystal Structure Torsion Angles (deg) and Ring Planarity for Oligothienyl−Ru(II) Complexes **2a**, **4a**, **4b**, and **6**·$2H_2O$·$^1/_2CH_2Cl_2$

(a) Crystallographic Data

	2a	**4a**	**4b**	**6**·$2H_2O$·$^1/_2CH_2Cl_2$
formula	$C_{34}H_{30}ORuClS_3P$	$C_{66}H_{42}BF_{24}OPRuS_3$	$C_{64}H_{38}BF_{24}OPRuS_3$	$C_{64}H_{50}O_2Ru_2Cl_2S_6P_2$·$2H_2O$·$^1/_2CH_2C_{l2}$
FW	718.29	1546.03	1517.98	1462.95
crystal system	triclinic	triclinic	triclinic	triclinic
space group	*P*-1 (No. 2)	*P*-1	*P*-1	*P*-1 (No. 2)
color, habit	yellow, plate	yellow, block	yellow, plate	yellow, columnar
a, Å	9.932(2)	13.6821(3)	12.2724(2)	11.2287(6)
b, Å	13.266(3)	15.4088(2)	13.6667(2)	16.1477(9)
c, Å	13.482(3)	17.4920(3)	21.3680(3)	18.7005(10)
α, deg	68.788(4)	103.8463(2)	84.7148(7)	77.5596(10)
β, deg	72.794(4)	94.7346(7)	81.0736(9)	79.9085(10)
γ, deg	72.088(4)	110.1334(8)	86.8583(5)	86.6928(10)
V, Å^3	1541.3(6)	3306.33(12)	3522.48(10)	3259.2(3)
dimensions, mm	0.25 × 0.25 × 0.05	0.30 × 0.30 × 0.20	0.30 × 0.30 × 0.25	0.59 × 0.11 × 0.04
temp, K	153(1)	198(2)	198(2)	153(1)
Z	2	2	2	2
R(*F*)[a]	*R*1 = 0.048	*R*1 = 0.0514	*R*1 = 0.1097	*R*1 = 0.072
	w*R*2[b] = 0.118	w*R*2[c] = 0.1166	w*R*2[c] = 0.2666	w*R*2[b] = 0.172
	[$I > 3\sigma(I)$]	[$I > 2\sigma(I)$]	[$I > 2\sigma(I)$]	[$I > 3\sigma(I)$]
GOF on F^2	1.48	1.009	1.384	3.25

(b) Crystal Structure Torsion Angles and Ring

complex	ring number[d]	ring planarity,[e] Å	deviation of S from plane, Å[f]	ring connectivity	torsion angle, deg
2a	1	0.0041	0.0168	1−2	19.80
	2	0.0055	0.0182	2−3	2.56
	3	0.0091	0.0114	1−3	17.25
4a	1	0.0158	0.0687	1−2	21.09
	2	0.0044	0.0059	2−3	32.47
	3	0.0058	0.0252	1−3	50.62
4b	1	0.0114	0.0496	1−2	10.09
	2	0.0085	0.0317	2−3	25.28
	3	0.0121	0.0193	1−3	19.03
6	1	0.0125	*g*	1−2	14.34
	2	0.0080	0.0320	2−3	14.10
	3	0.0065	0.0256	3−4	13.75
	4	0.0079	0.0191	4−5	30.47
	5	0.0059	0.0143	5−6	23.47
	6	0.0161	*g*	1−6	20.45

[a] $R1 = \sum||F_o| - |F_c||/\sum|F_o|$; $wR2 = [\sum(w(F_o^2 - F_c^2)^2)/\sum w(F_o^2)^2)]^{1/2}$. [b] $w = 1/(\sigma^2F^2)$. [c] $w = 1/[\sigma^2(F_o^2) + (aP)^2 + bP]$, $P = [2F_c^2 + \mathrm{Max}(F_o^2,0)]/3$. [d] The ring number in **2a**, **4a**, and **4b** is defined such that ring one is the terminal ring closest to the methylene substituent, and the numbering of the remaining rings is consecutive. For **6**, the ring number corresponds to the number of the sulfur atom. [e] Mean deviation of the atoms from the plane defined by the five thienyl atoms of each ring. [f] Deviation of the S atom from the plane defined by the four thienyl carbons in each ring. [g] Rings are disordered.

Electrochemistry of 4a and 5a. The cyclic voltammetry of **4a** in CH_2Cl_2/0.1 M *n*-Bu_4NPF_6 exhibits a chemically reversible, one-electron, terthienyl-based oxidation/reduction wave at $E_{1/2}$ = 735 mV, Figure 3, and an irreversible oxidation at 1180 mV (not shown). All electrochemical data are internally referenced and reported versus FcH/FcH^+ unless noted otherwise, FcH = (η^5-C_5H_4)Fe(η^5-C_5H_5). The first wave is attributed to ligand-centered oxidation/reduction of **4a** and reversible formation of the radial cation **4a**$^+$. The one-electron nature of this process was confirmed by variable scan rate cyclic voltammetry and variable spin rate rotating disk electrode experiments.[14] The second oxidation is assigned to terthienyl-centered dication formation. These assignments were made on the basis of a comparison of the cyclic voltammetry data for **4a** to the cyclic voltammograms of model compounds.[19,20] For example, [Cp(CO)(P(CH_2CH_3)Ph_2)Ru(CH_3CN)]BF_4,[14] a model complex for the metal center in **4a**, is oxidized irreversibly at 1335 mV in CH_3CN/CH_2Cl_2 (1:1). Additionally, 5,5″-dimethylterthiophene,[34] a model compound for the terthienyl-centered electrochemistry of **4a**, exhibits two reversible oxidation/reduction waves with $E_{1/2}$ values of 520 and 1020 mV, respectively, in CH_2Cl_2/0.1 M *n*-Bu_4NPF_6. These values are consistent with those reported by Mann and co-workers for this same compound in CH_3CN/*n*-Bu_4NBF_4[19] and for 3′,4′-dibutyl-5,5″-diphenylterthiophene in CH_2Cl_2/*n*-Bu_4NPF_6.[20]

Upon chloride abstraction from **2a** to yield **4a**, the $E_{1/2}$ for the terthienyl-based radical cation formation increases by 225 mV due to a combination of effects, including the binding of the oligothienyl backbone to a cationic metal and any changes in the electronic nature of the thienyl rings due to metal−sulfur binding (vide infra). Concomitantly, the metal oxidation potential increases as expected for a cationic complex and is outside the potential window of the solvent/supporting electrolyte solution, Table 2.

When CH_3CN is added to a CH_2Cl_2 solution of **4a**, the complex is converted to [Cp(CH_3CN)RuCO(3′-(2-diphenylphosphinoethyl)-5,5″-dimethyl-2,2′:5′,2″-terthiophene)][B(C_6H_3-3,5-(CF_3)$_2$)$_4$] (**5a**), a CH_3CN adduct formed via displacement of the η^1-terthienyl moiety from the Ru center by CH_3CN. A cyclic voltammogram of **5a** exhibits two waves. The lower potential wave is assigned to reversible radical cation formation ($E_{1/2}$ = 535 mV), and the higher potential wave is assigned to irreversible dication formation (E_{pa} = 960 mV), Table 2. The first wave for **5a** has an $E_{1/2}$ value that is 200 mV lower than the first $E_{1/2}$ for **4a**, and this difference allows one to estimate the *quantitative* increase in the Ru(II) binding constant (*K*) for

Table 2. Cyclic Voltammetry[a] and UV−Vis Spectroscopy[b] of Oligothienyl−Ru(II) Complexes

complex	$E_{1/2}$ (radical cation)/mV vs FcH/FcH$^+$ ($E_{pa} - E_{pc}$)	$E_{1/2}$ (Ru(II/III))/mV vs FcH/FcH$^+$ ($E_{pa} - E_{pc}$)	$E_{1/2}$ (dication)/mV vs FcH/FcH$^+$ ($E_{pa} - E_{pc}$)	UV−vis $\pi-\pi^*$ transition λ_{max}/nm
2a	510 (70)	680 (70)	945 (70)	353
4a	735 (100)	*c*	1180 (E_{pa})	352, 420 (sh)
5a	535 (70)	*c*	960 (E_{pa})	351
2b	∼735 (E_{pa})[d,e]	*d*	*d*	344
4b	∼765 (E_{pa})[d,e]	*c*	*d*	340, 420 (sh)
5b	∼685 (E_{pa})[d,e]	*c*	*d*	341
6	365 (70)	645[f] (120)	645[f] (120)	430
7	520 (60)	*c*	820 (60)	456
8	415 (60)	*c*	605 (60)	430
poly-**4b**	typical $E_{1/2} = 540$ mV[e]			

[a] In 0.1 M *n*-Bu_4NPF_6 in CH_2Cl_2 and referenced vs internal FcH/FcH$^+$ unless noted otherwise. [b] In CH_2Cl_2. [c] Outside of solvent window. [d] Cyclic voltammogram response convoluted by simultaneous polymerization. [e] In 0.1 M $LiB(C_6F_5)_4{\cdot}Et_2O$ in CH_2Cl_2. [f] Waves overlap.

CH_3CN upon terthienyl-based oxidation. From the Nernst equation, $\Delta E_{1/2} = (RT/nF)\ln(K_{ox}/K_{red})$,[41] or $K_{ox}/K_{red} = 2.4 \times 10^3$. Alternatively, this ratio may be viewed as a measure of the decrease in binding constant of the terthienyl RHL for Ru(II) that accompanies ligand-based oxidation.

FT-IR Spectroelectrochemistry of 4a. Spectroelectrochemical FT-IR experiments of **4a** in CH_2Cl_2/0.1 M $NaBAr_4'$ provide insight into the influence of terthienyl-based oxidation on the electronic properties of the bound Ru(II) center. The ν_{CO} of a metal carbonyl complex can be an excellent spectroscopic indicator of the amount of electron density at a metal center; as the electron-richness of a metal center decreases, CO stretching frequencies typically increase.[42] By setting the potential of the working electrode in a spectroelectrochemical cell to 600 mV vs an Ag wire (approximately 800 mV vs FcH/FcH$^+$, external reference), ligand-based oxidation of **4a** can be effected. This oxidation results in formation of **4a**$^+$ with a concomitant shift in the CO stretching frequency to a higher wavenumber than for **4a**. This change can be visualized through difference spectra obtained by subtracting the initial spectrum of **4a** from the spectra acquired at 600 mV vs an Ag wire as a function of time. The difference spectrum obtained in this way for **4a** has a band with a positive peak at 2011 cm^{-1} and a negative peak at 1992 cm^{-1}. The absolute intensity values of the positive peak at 2011 cm^{-1} and the negative peak at 1992 cm^{-1} increase with time and correspond to a buildup of **4a**$^+$ and a loss of **4a**, respectively, Figure 4a. Reduction of **4a**$^+$ for 15 min at 0 mV reverses the process and results in a flat line in the difference spectrum, indicating complete chemical reversibility, Figure 4e.

To determine how spectroelectrochemical difference bands relate to actual FT-IR bands of new products, model difference spectra were simulated from an authentic spectrum of **4a**. First, the *x*-axis of the spectrum of **4a** was systematically altered to generate model spectra with ν_{CO} values ranging from 1995 to 2025 cm^{-1}. Second, the difference spectra between these model spectra and the original spectrum of **4a** were obtained. These simulations show that if the separation between the peak frequencies of the spectra of **4a** and a new product is less than 20 cm^{-1}, the peak frequencies in the experimental difference spectra will not accurately represent the values of the actual ν_{CO} bands. (The full width at half-maximum for the spectrum of **4a** is 19.3 cm^{-1}). Additional simulations show that the peak frequencies in the experimental difference spectra should be independent of the extent of product formation. From comparison of the difference spectra obtained experimentally and by these simulations, it is estimated that the actual band of **4a**$^+$ is 2006−2011 cm^{-1}, or 10−15 cm^{-1} higher than the ν_{CO} of **4a**.

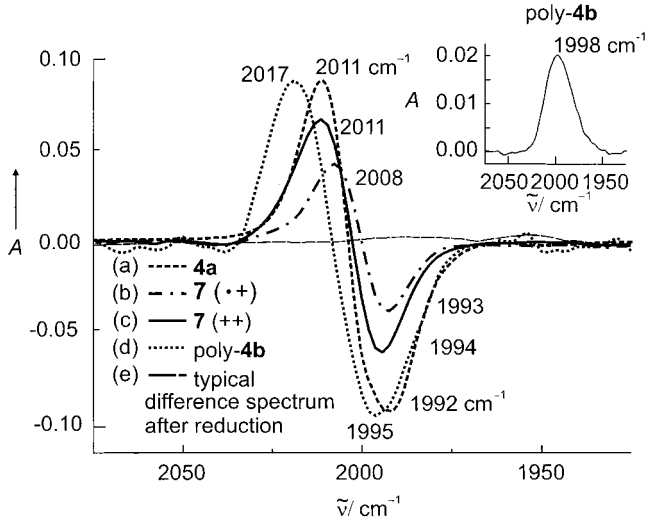

Figure 4. FT-IR spectroelectrochemical experiments: (a) 0.006 M **4a**, 0.03 M $NaBAr'$, CH_2Cl_2, Pt mesh counter, Ag wire quasi-reference, and Au minigrid working electrodes. Potential held at 600 mV vs Ag wire for 9 min. (b and c) 0.005 M **7**, 0.04 M $LiB(C_6F_5)_4{\cdot}Et_2O$, CH_2Cl_2, Pt wire counter, Ag/AgCl reference, Au minigrid working electrode. (b) Potential held at 700 mV vs FcH/FcH$^+$ for 2 min. (c) Potential held at 1100 mV vs FcH/FcH$^+$ for 2 min. (d) Poly-**4b**, 0.04 M $LiB(C_6F_5)_4{\cdot}Et_2O$, CH_2Cl_2, Pt mesh counter, Ag/AgCl reference electrode, derivatized Au working electrode. Potential held at 800 mV vs FcH/FcH$^+$ for 2 min. (e) Typical difference spectrum after reduction of the ligand in experiments a−d.

The magnitude of the change in ν_{CO} observed upon ligand-based oxidation in **4a** is substantial, considering that direct spectroelectrochemical oxidation of the Ru(II) center in isoelectronic $Cp(CO)(P(CH_2CH_3)Ph_2)RuCl$ results in a 90 cm^{-1} shift in ν_{CO} (ν_{CO}: [Ru(II)] = 1955 cm^{-1}; [Ru(III)] = 2045 cm^{-1}).[14] This change in ν_{CO} recorded upon metal-centered oxidation suggests that terthienyl-centered oxidation in **4a** corresponds to the removal of approximately 11−17% of an electron from the Ru center in terms of electronic change at the metal center.

Synthesis and Characterization of 4a$^+$ and 5a$^+$. In addition to the electrochemical and spectroelectrochemical formation of **4a**$^+$ and **5a**$^+$, these complexes can be prepared by bulk electrochemical oxidation of **4a** and **5a**, respectively, in a two-compartment cell. The deep-blue paramagnetic complexes have been characterized by FT-IR, UV−vis, and EPR spectroscopies (see Supporting Information). For **4a**$^+$, the ν_{CO} band in the FT-

(41) Miller, S. R.; Gustowski, D. A.; Chen, Z.-H.; Gokel, G. W.; Echegoyen, L.; Kaifer, A. E. *Anal. Chem.* **1988**, *60*, 2021−2024.

(42) Collman, J. P.; Hegedus, L. S.; Norton, J. R.; Finke, R. G. *Principles and Applications of Organotransition Metal Chemistry*; University Science Books: Mill Valley, CA, 1987.

Scheme 3

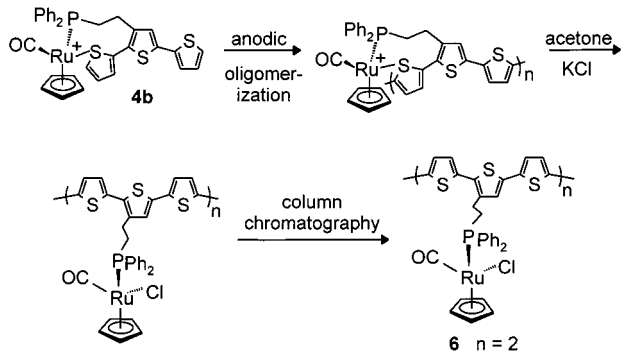

IR spectrum is at 2006 cm^{-1}, consistent with the range of values determined by simulation of the difference spectra resulting from spectroelectrochemical oxidation of **4a**. In contrast, for $\mathbf{5a}^+$, the ν_{CO} band in the FT-IR spectrum remains unchanged from that of **5a**, as expected due to the lack of direct communication between the terthienyl moiety and the metal center in these complexes. After oxidation of **4a** and **5a**, the solution UV−vis spectra of the resulting materials typically exhibit broad bands with λ_{max} values of 656 and 685 nm, respectively, Table 2.[43] These spectra differ significantly from the reported UV−vis spectrum of the radical cation of 5,5″-dimethylterthiophene (λ_{max} = 572 and 880 nm in CH_3CN/0.1 M *n*-Bu_4NBF_4),[44] and its π dimer (λ_{max} = 466, 708, and 868 nm).[23] The widths of the transitions for $\mathbf{4a}^+$ and $\mathbf{5a}^+$ could be due, in part, to the π-dimerization of $\mathbf{4a}^+$ and $\mathbf{5a}^+$.

Synthesis and Characterization of a Neutral Dinuclear Complex, 6. To better understand the properties of the Ru(II)−terthienyl complexes reported herein, dimeric analogues of these complexes were synthesized. Complex **6**, a dimeric analogue of **2b**, can be prepared by first oligomerizing **4b** electrochemically in CH_2Cl_2/$LiB(C_6F_5)_4$·Et_2O by repeatedly scanning the potential of the working electrode between 0 and 900 mV vs an Ag wire in a cyclic voltammetry experiment, Scheme 3. This oxidation yields soluble analogues of **4b** with *n* (number of repeat units) values greater than 1. Removal of the methylene chloride from the solution of oligomers, addition of acetone and KCl (10 equiv), and stirring the resulting mixture for 1 week under ambient conditions yields a solution of chloride adducts of the initial metal complexes. From these oligomers, **6** can be isolated in 66% yield by preparative scale thin-layer chromatography using an alumina support and methylene chloride as the eluent.

Complex **6** has been fully characterized in solution and in the solid state, and its solution spectroscopic data are consistent with its proposed structural formulation. For example, the ν_{CO} band in the FT-IR spectrum of **6** is at 1955 cm^{-1}, which compares well to the ν_{CO} band for **2b**. Also, the λ_{max} in the UV−vis spectrum of **6** is at 430 nm, which compares well to a reported λ_{max} for sexithiophene (432 nm in $CHCl_3$).[45] The $\pi-\pi^*$ transition for **6** (λ_{max} = 430 nm) is at lower energy than the $\pi-\pi^*$ transition for **2b** (λ_{max} = 344 nm), as expected for an oligomer with longer conjugation length. The $E_{1/2}$ value associated with radical cation formation and reduction in **6** (365 mV) is much lower than the one-electron oxidation/reduction of **2a**, Table 2. This decrease in $E_{1/2}$ is due to an increase in conjugation which results from the increased number of thienyl rings in **6** compared to **2a**. Dication formation for **6** also occurs at a lower potential than for **2a** and overlaps the metal-centered redox process of **6** ($E_{1/2,apparent}$ = 645 mV, two-electron process).

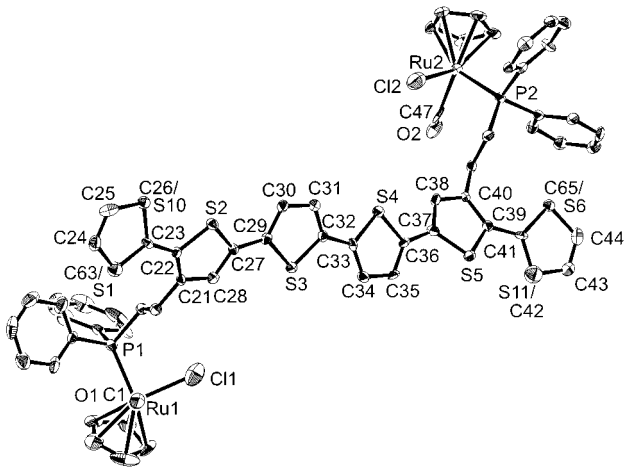

Figure 5. ORTEP diagram of $\mathbf{6}\cdot 2H_2O\cdot {}^1/_2CH_2Cl_2$ (hydrogen atoms are omitted for clarity). Thermal ellipsoids are drawn at 30% probability.

Solid-State Structure of $\mathbf{6}\cdot 2H_2O\cdot {}^1/_2CH_2Cl_2$. A crystal of $\mathbf{6}\cdot 2H_2O\cdot {}^1/_2CH_2Cl_2$ suitable for a single-crystal X-ray diffraction study was grown by slow diffusion of pentane into a solution of **6** in CH_2Cl_2. The crystal structure of $\mathbf{6}\cdot 2H_2O\cdot {}^1/_2CH_2Cl_2$ shows that there are two tetrahedral metal centers bound via methylene arms to a sexithienyl backbone and that the thienyl rings have an antiparallel arrangement with all α linkages, Figure 5 and Table 1 (see Supporting Information). The terminal rings in the crystal structure of $\mathbf{6}\cdot 2H_2O\cdot {}^1/_2CH_2Cl_2$ were modeled as rotationally disordered with an occupancy distribution of 50/50 and 35/65 parallel and antiparallel ring configurations for rings 1 and 6, respectively. The disordered sulfur and carbon atoms of these rings were refined with g\tied isotropic thermal parameters. Similar disorder in terminal thienyl rings in the crystal structures of substituted oligothiophenes has been reported previously.[46] The structure contains disordered H_2O and CH_2Cl_2 molecules, which were refined isotropically, while the non-hydrogen atoms in the main molecule were refined anisotropically. The crystal structure of $\mathbf{6}\cdot 2H_2O\cdot {}^1/_2CH_2Cl_2$ shows that the terminal rings of **4b**, which are not bound to Ru, are covalently linked in the oxidative coupling reaction which forms **6**. The isolation of this connectivity isomer in 66% yield suggests that this connection of the thienyl rings is the preferred terthienyl linkage in the electrochemical oligomerization of **4b**. This preference is most likely due to a combination of steric and electronic factors which places the most available unpaired electron density on the terminal, unbound thienyl ring in the monomer upon ligand-based oxidation. The C−S bond lengths in the rings of **6** are not elongated as in the rings of **4a** and **4b**, evidence that this elongation is due to oligothienyl−Ru binding. Additionally, the planarities of the thienyl rings in $\mathbf{6}\cdot 2H_2O\cdot {}^1/_2CH_2Cl_2$ are comparable to those of **2a**, **4a**, and **4b**.

The torsion angles between adjacent, individual rings in the solid-state structures of **2a**, **4a**, **4b**, and **6** range from 2.56° to 32.47° and are summarized in Table 1b. These torsion angles are greater than the torsion angles observed in unsubstituted

(43) Although the UV−vis spectrum of a typical sample of $\mathbf{4a}^+$ exhibits a broad band at 656 nm, sometimes this band is comprised of two bands at 579 nm and a broad band with λ_{max} at approximately 654 nm.

(44) In our hands, the UV−vis spectrum of 5,5″-dimethylterthiophene in methylene chloride/0.1 M *n*-Bu_4NPF_6 has two transitions with λ_{max} values of 581 and 889 nm.

(45) Van Pham, C.; Burkhardt, A.; Shabana, R.; Cunningham, D.; Mark, H.; Zimmer, H. *Phosphorus, Sulfur Silicon* **1989**, *46*, 153−168.

(46) Herrema, J. K.; Wildeman, J.; van Bolhuis, F.; Hadziioannou, G. *Synth. Met.* **1993**, *60*, 239−248.

oligothiophenes (6−9° for α-terthiophene,[47] less than 1° for α-octithiophene,[48] and less than the esd for sexithiophene[49]) but are comparable to the torsion angles observed in other previously reported substituted oligothiophenes (5−11° in a dialkyl-substituted sexithiophene[46] and as large as 37.4° in a terminally substituted sexithiophene[49]). Since **2a**, **4a**, **4b**, and **6** all have comparable torsion angles, it appears that η^1-thienyl binding of the oligothienyl ligand to the metal center does not cause increases in the torsion angles compared to "free" oligothienyl moieties. Significantly, all of the inter-ring dihedral torsion angles in **2a**, **4a**, **4b**, and **6** are less than 40°, the angle below which ab initio calculations on polythiophene show that the torsion does not significantly affect the electronic properties of the polymer.[50]

Synthesis and Characterization of a Cationic Dinuclear Complex, 7. When **6** is treated with $LiB(C_6F_5)_4 \cdot Et_2O$ for 1 week in methylene chloride, **7** forms in quantitative yield, eq 1. Complex **7** was characterized in solution, and its solution

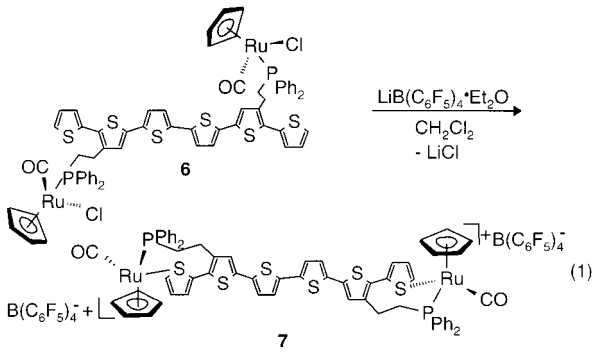

spectroscopic data are consistent with its proposed structural formulation. The FT-IR spectrum of **7** in CH_2Cl_2 exhibits a ν_{CO} band at 1996 cm^{-1}, consistent with the data acquired for **4b**. The UV−vis spectrum for **7** shows evidence for a $\pi-\pi^*$ transition with $\lambda_{max} = 456$ nm in CH_2Cl_2, consistent with this analogous transition for other sexithiophene derivatives[51] but shifted to lower energy compared to **6**. Although binding of the Ru centers to the thienyl S atoms in **7** is expected to remove electron density from the sexithienyl ligand, which should raise the energy of the $\pi-\pi^*$ transition, the observed shift is likely due to the reduction in rotational ring disorder that the metal−thienyl interaction provides, as observed for other terthienyl−Ru(II) complexes.[9]

Electrochemistry of 7 and 8. The cyclic voltammogram of **7** shows two reversible oxidation/reduction waves with $E_{1/2}$ values of 520 and 820 mV, respectively, Figure 6. The first wave for this complex is associated with ligand-based, one-electron oxidation to form a radical cation, and the second wave is attributed to dication formation by comparison with the cyclic voltammetry for **4a** and the cyclic voltammogram reported for didodecylsexithiophene ($E° = 0.34$, 0.54 V vs FcH/FcH^+).[52] The $E_{1/2}$ for radical cation formation/reduction increases by 155 mV from **6** to **7** due to Ru bonding to the S atom in the latter

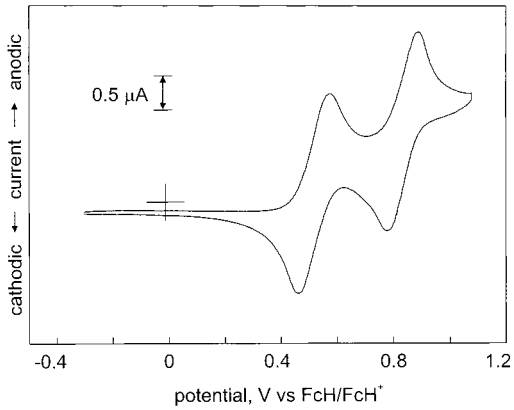

Figure 6. Cyclic voltammogram of **7** in CH_2Cl_2/0.1 M n-Bu_4NPF_6 using an Au working electrode, Pt mesh counter electrode, and Ag wire quasi-reference electrode at a scan rate of 100 mV/s.

complex; the $E_{1/2}$ for dication formation in **7** is also higher (approximately 175 mV) than the potential observed for dication formation for **6**. Additionally, the metal-centered oxidation of **7** is no longer accessible in CH_2Cl_2; this increase in the potential for the metal-centered oxidation in **7** relative to metal-centered oxidation in **6** is expected due to the replacement of an anionichalide ligand with a neutral thienyl moiety. Significantly, the waves associated with oxidation of the ligand-based radical cation to the dication are reversible in the dinuclear, sexithienyl complexes (**7**, **8**) but irreversible in the mononuclear analogues (**4a**, **5a**) due to the increased stability of the cations on the longer oligothiophene backbones.

By dissolving **7** in CH_3CN, the bis-CH_3CN adduct of **7**, complex **8**, can be prepared in quantitative yield. This new complex has been characterized in solution, and its spectroscopic data are consistent with its proposed formulation (see Experimental Section). The cyclic voltammogram of **8** shows two reversible waves with $E_{1/2}$ values of 415 and 605 mV, associated with the formation of radical cation and dication, respectively. Significantly, the $E_{1/2}$ value associated with radical cation formation in **8** is 105 mV lower in potential than the $E_{1/2}$ for **7**. Therefore, the binding constant (K) of **7** for CH_3CN increases by a factor of 60 upon one-electron, ligand-based oxidation as calculated from the Nernst equation. This binding constant increase is smaller than the change in CH_3CN binding constant observed for the terthienyl complex **4a** upon its oxidation. This trend is expected for a single hole on an oligothiophene backbone—if the hole is delocalized over more thienyl rings, or able to move farther from the metal center, the electronic change at the metal center will be smaller.

FT-IR Spectroelectrochemistry of 7. FT-IR spectroelectrochemistry of **7** was performed in CH_2Cl_2/0.04 M $LiB(C_6F_5)_4 \cdot Et_2O$ by techniques analogous to those used for the spectroelectrochemical experiments for **4a**. Setting the working electrode potential to 700 mV vs FcH/FcH^+ (externally referenced) and subtracting the initial spectrum from the resulting spectrum yields a difference spectrum with a positive peak at 2006 cm^{-1} (associated with an increase in 7^+ upon oxidation of **7**) and a negative peak at 1992 cm^{-1} (corresponding to loss of **7** upon oxidation), Figure 4c. These difference peaks correspond to an actual FT-IR band of 2000−2006 cm^{-1} for 7^+, as determined by simulation of the difference spectra as previously described. Upon oxidation of **7** at 1100 mV, which is past the second oxidation potential of **7**, the difference band exhibits a positive peak at 2011 cm^{-1} (corresponding to 7^{++} and 7^+) and a negative peak at 1994 cm^{-1} (corresponding to loss of **7** upon oxidation), Figure 4b. Simulation of the spectra is an insufficient method

(47) van Bolhuis, F.; Wynberg, H.; Havinga, E. E.; Meijer, E. W.; Staring, E. G. J. *Synth. Met.* **1989**, *30*, 381−389.
(48) Fichou, D.; Bachet, B.; Demanze, F.; Billy, I.; Horowitz, G.; Garnier, F. *Adv. Mater.* **1996**, *8*, 500−504.
(49) Yassar, A.; Garnier, F.; Deloffre, F.; Horowitz, G.; Ricard, L. *Adv. Mater.* **1994**, *6*, 660−663.
(50) Brédas, J. L.; Street, G. B.; Thémans, B.; André, J. M. *J. Chem. Phys.* **1985**, *83*, 1323−1329.
(51) Martinez, F.; Voelkel, R.; Naegele, D.; Naarmann, H. *Mol. Cryst. Liq. Cryst.* **1989**, *167*, 227−232.
(52) Bäuerle, P.; Segelbacher, U.; Gaudl, K.-U.; Huttenlocher, D.; Mehring, M. *Angew. Chem., Int. Ed. Engl.* **1993**, *32*, 76−78.

to assign the frequency of the actual band for $\mathbf{7}^{++}$ from the difference band because the difference spectrum arises from a multicomponent system. However, this FT-IR change upon formation of the dication from the radical cation is consistent with a more highly charged oligothienyl backbone which withdraws more electron density from the bound Ru(II) centers. Reduction of the doubly oxidized complex at −150 mV for 15 min shows the decrease in the absolute intensities of the FT-IR difference peaks associated with the oxidized products, confirming the reversibility of these electrochemical reactions, Figure 4e.

Synthesis and Characterization of $\mathbf{7}^+$ and $\mathbf{8}^+$. Bulk electrochemical oxidation of **7** and **8** allows for the preparation of $\mathbf{7}^+$ and $\mathbf{8}^+$, respectively, which have been characterized by UV−vis and EPR spectroscopies (see Supporting Information). The spectra of the materials resulting from the one-electron oxidation of **7** and **8** have bands at 762 (680 nm, sh) and 760 nm (700 nm, sh), respectively. These spectra compare well with the reported spectrum for oxidized didodecylsexithiophene, which exhibits a band at 775 nm and a shoulder at 685 nm; the high-energy shoulder was attributed to the formation of the π-dimer.[52] By analogy, the shoulders observed in spectra of $\mathbf{7}^+$ and $\mathbf{8}^+$ are attributed to the diamagnetic π-dimer. The energies of the $\pi-\pi^*$ transitions for sexithienyl complexes $\mathbf{7}^+$ and $\mathbf{8}^+$ are very similar, whereas the energies of the $\pi-\pi^*$ transitions for **7** and **8** differ by 26 nm.

The UV−vis spectra for **7**, $\mathbf{7}^+$, **8**, and $\mathbf{8}^+$ compare well with the spectra of previously reported sexithienyl compounds. For example, for unsubstituted oligothiophenes in $CHCl_3$, the $\pi-\pi^*$ transitions for quaterthiophene, pentathiophene, and sexithiophene are at 390, 416, and 434 nm, respectively.[51] The $\pi-\pi^*$ transitions for the corresponding quaterthiophene and sexithiophene radical cations are at 614 and 775 nm, respectively.[53] For another series of trimethylsilyl-terminated oligothiophenes, the quaterthienyl transition is at 394 nm, the pentathienyl transition is at 422 nm, and the sexithienyl transition is at 422 nm; the radical cation analogues are at 666, 743, and 779 nm, respectively.[27] Significantly, the absorption bands for $\mathbf{7}^+$ and $\mathbf{8}^+$ are inconsistent with the reported spectra for oxidized oligothiophenes with four rings, indicating that the binding of an oligothienyl ring to the Ru center does not remove that ring from conjugation with the unbound rings.

Synthesis and Characterization of a Polymeric Complex, Poly-4b. Poly-**4b** has been electrochemically deposited onto an Au foil electrode by electrochemically oxidizing **4b** in CH_2Cl_2/0.1 M $LiB(C_6F_5)_4 \cdot Et_2O$ in a cyclic voltammetry experiment. The characteristic oxidative peak for this terthienyl compound is observed at 765 mV vs FcH/FcH^+ (external reference), and the reversible oxidation/reduction wave for a typical deposited polymer has an $E_{1/2}$ value of 540 mV vs FcH/FcH^+. The specular reflectance FT-IR spectrum of poly-**4b** exhibits a single metal carbonyl band at 1998 cm^{-1} (fwhm = 34 cm^{-1}), which is almost identical in frequency to that of the monomer **4b** (1997 cm^{-1}). Since IR spectroscopy in this region probes the CO-containing Ru fragments, the similarity of the ν_{CO} of the polymer to that of the monomer suggests that all of the CO-containing Ru centers are electronically similar to the monomer. EDS shows, within experimental error, that the Ru:S ratio remains constant before and after polymerization (polymer, 1.47 ± 0.05; cast film of **4b**, 1.47 ± 0.16), suggesting that no appreciable leaching of the metal from the polymer occurs.[14] When poly-**4b** is immersed in a 0.04 M solution of $(CH_3)_3CNC$ in CH_2Cl_2 for 7 days, the resulting film exhibits two FT-IR bands, ν_{CN} = 2175 cm^{-1} and ν_{CO} = 2008 cm^{-1}. These bands are consistent with those of the isonitrile adduct (**9**) formed upon reaction of **4a** and $(CH_3)_3CNC$ (ν_{CN} = 2176 cm^{-1}, ν_{CO} = 2003 cm^{-1}) (vide infra). This reaction demonstrates the coordinative lability of the polymeric thienyl ligand and provides further evidence that the chemical nature of the film is similar to that of the monomer.

FT-IR Spectroelectrochemistry of Poly-4b. Although **4a** has only two and **7** has only three electrochemically accessible, stable oligothienyl oxidation states, poly-**4b** might be expected to have many due to the terthienyl repeat unit along the polymer backbone. Spectroelectrochemical experiments were performed on poly-**4b** by oxidizing the polymer, immobilized on a gold foil working electrode, at 800 mV (external reference vs FcH/FcH^+) in a three-electrode electrochemical cell, removing the electrode from the cell under potential control, and acquiring the specular reflectance FT-IR spectrum. Upon polyterthienyl-centered oxidation, an FT-IR difference band is observed with a positive peak at 2017 cm^{-1} and a negative peak at 1995 cm^{-1}, with a concomitant color change of the polymer from orange to blue, Figure 4d. This oxidation process can be electrochemically reversed, as evidenced by the flat difference spectrum obtained by subtracting the spectrum of poly-**4b** after re-reduction at 0 mV for 2 min from poly-**4b** before oxidation, Figure 4e. It is important to note that no changes in the FT-IR spectrum are observed until the application of this threshold potential and that continued increases in the absolute values of the positive and negative difference peaks at 2017 and 1995 cm^{-1}, respectively, are observed as the polymer is oxidized at potentials up to 300 mV past the threshold potential (i.e., higher oxidation potentials do not lead to a positive difference peak with a higher ν_{CO}).

Independently prepared films of poly-**4b** have difference bands associated with spectroelectrochemical oxidation with positive difference peaks which range from 2017 to 2011 cm^{-1}. However, all films exhibit the same qualitative behavior (i.e., a single difference band at a threshold oxidation potential). The value of the positive difference peak largely depends on the peak frequency and width of the initial spectrum of poly-**4b**. Simulation of the spectroelectrochemical difference spectra for several independently prepared films of poly-**4b** using their respective initial spectra shows that the actual ν_{CO} for each film of oxidized poly-**4b** is approximately 10 cm^{-1} greater than that for poly-**4b**, consistent with the changes observed upon oxidation of **4a** and **7**.

The intensity of the carbonyl band in poly-**4b** decreases reversibly by 30−40% upon polymer oxidation. Decreases in metal−carbonyl and −isocyanide stretching band intensities accompanying metal-centered oxidation processes have been noted in the literature for metal−carbonyl and −isocyanide complexes, respectively.[54−57] This effect has been explained in terms of the reduction in the metal-dπ to ligand-π^* back-bonding with increases in metal oxidation. This reduction decreases the amount of charge transferred to the CO or CN during the vibrational transition, thereby reducing the net dipole moment change during that transition. The decrease in carbonyl stretching band intensity upon ligand-centered oxidation in poly-**4b** shows that ligand-based oxidation, in addition to metal-based oxidation, can cause this effect.

(53) Caspar, J. V.; Ramamurthy, V.; Corbin, D. R. *J. Am. Chem. Soc.* **1991**, *113*, 600−610.

(54) Kettle, S. F. A.; Paul, I. In *Infrared Intensities of Metal Carbonyl Stretching Vibrations*; Stone, F. G. A., West, R., Eds.; Academic Press: New York, 1972; Vol. 10, pp 199−236.

(55) Noack, K. *Helv. Chim. Acta* **1962**, *45*, 1847−1859.

(56) Bullock, J. P.; Mann, K. R. *Inorg. Chem.* **1989**, *28*, 4006−4011.

(57) Brown, T. L.; Darensbourg, D. J. *Inorg. Chem.* **1967**, *6*, 971−977.

Probing the Reactivity of 4a with Small Molecules with Various Ligating Properties. To determine the oxidation-state-dependent reactivity of **4a**, its reactivity patterns were studied by a series of NMR tube reactions, eq 2. Addition of 44 equiv

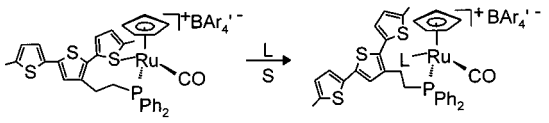

(2)

5a: L = CH_3CN, S = CD_2Cl_2
9: L = *t*-BuNC, S = CD_2Cl_2
10: L = acetone-d_6, neat
11: L = CO, S = acetone-d_6
12: L = ethylene, S = CD_2Cl_2
13: L = thiophene, neat

of CH_3CN to **4a** in CD_2Cl_2 at room temperature results in the overnight formation of the CH_3CN adduct, **5a**. The metal-bound CH_3CN in **5a** can be removed by heating **5a** to 100 °C in vacuo (<50 mTorr) for 5 days. Similarly, addition of 5 equiv of $(CH_3)_3CNC$ to **4a** in CD_2Cl_2 at room temperature for 12 days results in the formation of the isocyanide adduct, **9**. Complex **9** is substitutionally inert with respect to displacement of the bound $(CH_3)_3CNC$, even when it is heated to 100 °C in vacuo (<50 mTorr) for 5 days.

Acetone (100 equiv) does not react with **4a** in CD_2Cl_2 at room temperature. However, if **4a** is dissolved in neat acetone-d_6, approximately 9% of the complex is converted to the acetone-d_6 adduct (**10**), which was determined by integration of the two Cp resonances observed in the ^1H NMR spectrum of the mixture of **4a** and **10**. Removing the excess acetone in vacuo and redissolving the resulting solid in CD_2Cl_2 results in quantitative re-formation of **4a**.

Carbon monoxide (2−4 psi) does not react with **4a** in CD_2Cl_2 at room temperature nor under refluxing conditions. In comparison, CO reacts slowly with **4a** in acetone-d_6 at room temperature or at reflux temperature to form the CO adduct of **4a**, complex **11**. Heating **11** to 100 °C in vacuo (<50 mTorr) for 5 days does not result in its reconversion to **4a**. Ethylene (2−4 psi) does not react with **4a** in CD_2Cl_2 under ambient conditions, but it does react with **4a** to form an ethylene adduct (**12**) upon refluxing the same sample. This reaction can be reversed to re-form **4a** by heating a sample of **12** to 100 °C in vacuo (<50 mTorr) for 5 days.

Although 1 equiv of thiophene does not react with **4a** in CD_2Cl_2 or acetone-d_6, when **4a** is dissolved in 10 mL of neat thiophene for 1 day, an equilibrium is established between **4a** and the thiophene adduct of **4a** (**13**). The product distribution was characterized by ^1H and $^{31}P\{^1H\}$ NMR spectra obtained after the excess thiophene was removed in vacuo at room temperature and the resulting solid was dissolved in CD_2Cl_2. These spectra show a 1.1:1 ratio of **4a** to **13**. However, after the sample is allowed to sit at room temperature for 1 day, the bound thiophene is displaced from the metal coordination sphere to yield **4a** and metal-free thiophene exclusively. The mode of coordination for thiophene cannot be established conclusively due to overlap of the thienyl resonances associated with **4a** and **13** in the ^1H NMR spectrum of **4a** and **13**. It is likely, however, that the coordination is through the S atom, based on the coordination mode in very similar complexes[17] and the lack of resonances in the ^1H NMR spectrum at δ 3−3.5, which would be present for a complex with thiophene bound in an η^2 fashion.

Probing the Reactivity of $4a^+$. The reactivity of paramagnetic $4a^+$ with CD_3CN, acetone-d_6, 2,5-dideuteriothiophene, and ethylene-d_4 was examined by variable-temperature $^2H\{^1H\}$ NMR experiments. Deuterium NMR resonances are often sharper than ^1H NMR resonances when the compounds being studied are in the presence of paramagnetic species.[58] Since replacing hydrogen with deuterium in small molecule substrates is not expected to significantly impact the steric or electronic nature of the substrates, monitoring the $^2H\{^1H\}$ NMR spectrum of deuterated ligands in the presence of $4a^+$ provides a convenient way to examine the binding behavior of these ligands to the metal center. For these VT $^2H\{^1H\}$ NMR experiments, $4a^+$ was prepared by bulk oxidation of 15 mg of **4a** in a two-compartment electrochemical cell with $LiB(C_6F_5)_4 \cdot Et_2O$ as the supporting electrolyte. The resulting $4a^+$/electrolyte solution was loaded into an air-free NMR tube in 0.4 mL of CH_2Cl_2 with 1 μL of CD_2Cl_2 as an internal standard. The $^2H\{^1H\}$ NMR spectra of these solutions show only the CD_2Cl_2 reference at δ 5.32.

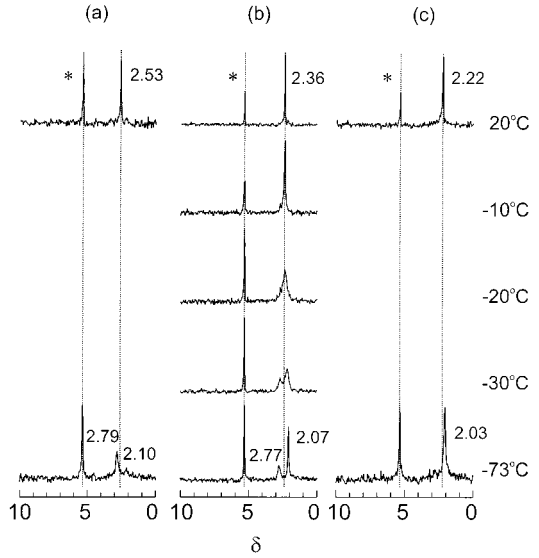

Figure 7. Variable-temperature $^2H\{^1H\}$ NMR spectra of $4a^+$ in CH_2Cl_2/CD_2Cl_2 for binding studies. Sequential addition of (a) 0.5 equiv of CD_3CN, (b) 1 equiv of CD_3CN, (c) 2 equiv of decamethylferrocene as reducing agent. The asterisk indicates CD_2Cl_2 internal reference.

After addition of 0.5 equiv of CD_3CN to a sample of $4a^+$ in CH_2Cl_2/CD_2Cl_2, a new resonance at δ 2.53 is observed, Figure 7. Significantly, this resonance is shifted downfield relative to the frequency observed for "free" CD_3CN in CH_2Cl_2 (δ 1.93). Upon cooling of the sample to −73 °C, the CD_3CN resonance splits into two separate resonances (δ 2.79, 2.10; downfield resonance more intense). After addition of a second half of an equivalent of CD_3CN to the sample at room temperature, the acetonitrile resonance moves upfield from δ 2.53 to 2.36. This change corresponds to more "free" CD_3CN in solution, which causes the weighted average to shift upfield. Upon cooling of the sample to −73 °C, the acetonitrile resonance splits into two resonances at δ 2.77 and 2.07. In this case, the upfield peak is more intense. These results are consistent with a chemical exchange process in which the CD_3CN is rapidly coordinating to and dissociating from the metal center coordination sphere; at room temperature the reaction is fast but at −73 °C the exchange is slow on the NMR time scale. Significantly, after addition of a reducing agent (decamethylferrocene, 2 equiv) to the solution at room temperature, all of the bound CD_3CN is released, as evidenced by VT $^2H\{^1H\}$ NMR spectroscopy. It should be noted that the spectra of control samples prepared with **4a** in place of $4a^+$ do not show significant temperature-dependent changes.

(58) Johnson, A.; Everett, G. W. *J. Am. Chem. Soc.* **1972**, *94*, 1419−1425.

Variable-temperature $^2H\{^1H\}$ NMR experiments designed to probe the reactivity of **4a**$^+$ with acetone-d_6, ethylene-d_4, and 2,5-dideuteriothiophene[59] were conducted analogously to those for CD_3CN. These studies indicate that **4a**$^+$ does not react with 1 equiv of ethylene-d_4, acetone-d_6, or 2,5-dideuteriothiophene under the conditions examined.

Discussion

We have developed a new redox-switchable hemilabile ligand (RHL), **1b**, which allows for the preparation of an isolable, mononuclear Ru(II) complex (**4b**) which can be oligomerized to yield dimers, oligomers, and surface-immobilized conducting polymer/metal hybrid materials. Also, model complex **4a**, a nonpolymerizable analogue of **4b**, has been studied electrochemically in solution under controlled conditions. These monomeric, oligomeric, and polymeric complexes have been used to evaluate the influence that redox-active thienyl-based ligands can have on the electronic and coordination environments of bound transition metal centers.

An important question to address is that of why the ligand-centered oxidation/reduction potentials increase for these oligothienyl complexes upon oligothienyl coordination to the Ru centers (Table 2): is the increase due to inductive effects associated with the cationic Ru centers or due to distortion of the metal-coordinated thienyl moieties, which results in decreased conjugation of the oligothienyl units that comprise the backbones of these ligands? Graf and Mann addressed this question for $[CpRu]^+$ fragments bound in an η^5 manner to oligothiophene backbones and concluded that the bonding of the $[CpRu]^+$ fragment to the oligothiophene effectively removes the metal-bound ring from π conjugation with the remaining unbound thiophene rings.[60] This article addresses this question for oligothiophenes bound in an η^1 fashion to Ru(II) metal centers.

If bonding between the metals and the oligothienyl groups in **4a** and **7** removes the bound rings from conjugation with the other thienyl rings, then the oxidation potentials of **4a** and **7** should be effectively those of bithienyl and quaterthienyl compounds, respectively. In several reported series of homologous oligothiophenes, the difference between bi- and terthienyl oxidation ranges from 150 to 250 mV, and the difference between quater- and sexithienyl oxidation ranges from 80 to 110 mV.[27,29,51] Thus, the differences in $E_{1/2}$ values observed for **4a** and **5a** (200 mV) and for **7** and **8** (105 mV) are consistent with removal of bound rings from conjugation upon terthienyl coordination to the Ru center. However, others have concluded that binding positive Ru centers in an η^6 fashion to phenyl groups of phenyl-terminated terthiophenes increases the terthienyl oxidation potential by 150 mV per metal center, mainly due to the effects of the positive Ru center.[60] Thus, the magnitudes of the changes in potential between **5a** and **4a** and between **7** and **8** also are consistent with inductive and electrostatic effects of the Ru cations. Therefore, cyclic voltammetry, alone, does not provide conclusive evidence regarding the reason for the ligand-centered oxidation/reduction potential increases upon oligothienyl−metal binding.

The energies of the $\pi-\pi^*$ transitions in the UV−vis spectra of **4a**, **5a**, **7**, **8**, and their oxidized forms, which are known to depend on the extent of ring conjugation in oligothiophene,[27,29,51] also can be used to address this question. Several factors influence the energy of oligothienyl $\pi-\pi^*$ transitions, including chain length (increased length leads to increased conjugation), steric interactions of substituents (steric interactions contribute to increased twisting of the rings and therefore decreased conjugation), and inductive electronic effects of the substituents. The spectra of complexes **5a** and **8**, in which the oligothienyl backbones are not coordinated to the metal centers, provide a comparison for the spectroscopy of the metal-bound oligothienyl complexes, **4a** and **7**, respectively. The λ_{max} values for **4a** and **5a**, and **7**$^+$ and **8**$^+$, are very similar to each other, respectively, suggesting that metal center binding does not significantly alter the extent of ring conjugation for these complexes. Thus, the combination of electrochemistry and UV−vis spectroscopy for these complexes suggests that metal center binding of the oligothienyl ligands primarily increases the ligand-based oxidation potentials due to the electronic influence of the positively charged metal centers.

The spectroelectrochemistry of **7** compared to that of **4a** shows that by increasing the length of the oligothienyl unit, additional ligand-centered oxidations become electrochemically accessible. Complex **7** provides an example of how sequential oxidations can result in successive increases in CO stretching frequency and, therefore, electronic changes at the metal center. Note that for the dimer (**7**), two, one-electron oxidation processes are required to effect a change in electronic character at the Ru center comparable to the change observed for a single, one-electron oxidation of the monomer (**4a**). Additionally, the fact that the CO stretching frequency of **7**$^+$ is lower than that of **4a**$^+$ implies that the charge does not remain unsymmetrically localized in **7**$^+$, which could result in one metal center feeling the doping level equivalent to that in **4a**$^+$ and one metal center remaining unaffected (and thus silent by difference spectroscopy). This observation indicates that the charge is delocalized over multiple rings in **7**$^+$. However, it is not known from these experiments whether the extent of delocalization of the hole is over three rings in the monomer and six rings in the dimer, or over two rings in the monomer and the four central rings in the dimer. Either explanation is consistent with the observed results for the spectroelectrochemical oxidation of **4a** and **7**.

Poly-**4b** provides additional insight into the degree of localization in these materials. In the FT-IR spectroelectrochemistry of poly-**4b**, a single quantized change in the ν_{CO} band is observed upon oxidation of the polymer backbone. Although several groups, including ours, have suggested that metal-conducting polymer complexes might give access to systems with tunable electrochemical properties based on extent of oxidation,[2−4] for this system, we do not observe gradual shifts in CO stretching frequency to higher energy as poly-**4b** is oxidized to higher potentials. These results are consistent with a model in which the charged Ru fragment causes the electron holes produced during oxidation of the polymer backbone to remain localized on the uncomplexed thienyl rings, at least on the time scale of the FT-IR experiment. The polymer consists of monomer units connected in ring 1−ring 1, ring 1−ring 3, and ring 3−ring 3 (as in **7**) manners (Figure 8); each connection provides for slightly different physical properties. However, the average effect in the polymer film is such that localization essentially transforms what ordinarily might be considered a delocalized conducting polymer into a string of monomers, giving rise to a single change in the spectroelectrochemical response at the potential capable of causing oxidation of these units. Consistent with this model, **7**$^+$ has a lower energy FT-IR band than **4a**$^+$ because in **7**$^+$ the electron hole is delocalized over the four internal rings not bound to Ru.

This article also addresses the design of polymeric RHL complexes for controlled small-molecule uptake and release.

(59) Delabouglise, D.; Garreau, R.; Lemaire, M.; Roncali, J. *New J. Chem.* **1988**, *12*, 155−161.

(60) Graf, D. D.; Mann, K. R. *Inorg. Chem.* **1997**, *36*, 150−157.

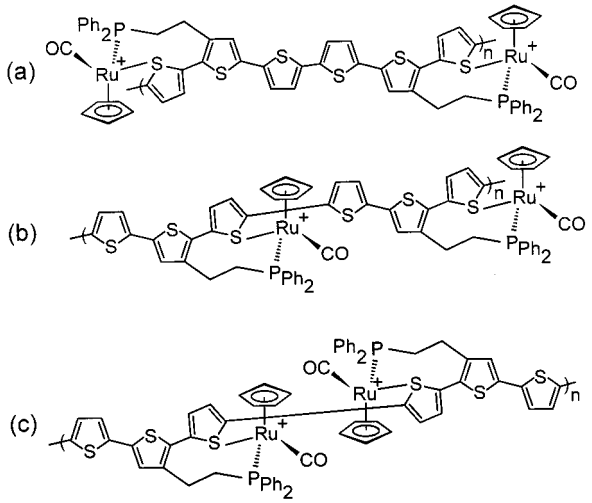

Figure 8. Three possible monomer linkages within poly-**4b**: (a) ring 3−ring 3, (b) ring 1−ring 3, and (c) ring 1−ring 1.

To successfully realize redox-controlled molecular uptake and release utilizing RHL-controlled metal center coordination sites, several requirements (ideally) must be achieved: (1) target substrates should not react with the RHL−metal complex in its reduced state, (2) target substrates should react (quickly) with the oxidized form of the RHL−metal complex to yield a metal−substrate adduct, and (3) target substrates should dissociate (quickly) from the metal center coordination sphere upon reduction of the RHL−metal complex, Scheme 1. Additionally, all complexes generated in this cycle must be chemically stable with respect to each other, the solvent, and the target substrate. For example, complexes of terthienyl-based redox-active ligands cannot be used with nucleophilic solvents or target substrates, including water, alcohols, and amines due to the ability of these nucleophiles to react with the oxidized form of the terthienyl ligand. These requirements necessitate a careful balance between the thermodynamic and kinetic factors which influence the oxidation-state-dependent binding properties of RHL−metal complexes when designing complexes for molecular uptake and release of target substrates.

Thermodynamic and kinetic factors govern the molecular uptake and release properties of these complexes. A comparison of the cyclic voltammogram of **4a** to that of **5a** shows that the binding constant of the metal center for CH_3CN increases by a factor of 2×10^3 upon ligand-centered oxidation, and the analogous experiments for **7** and **8** show that the binding constant increases by a factor of 60. This comparison demonstrates that the thermodynamic perturbation on the oligothienyl backbone, in both cases, is significant upon ligand-based oxidation.

$^2H\{^1H\}$ NMR experiments were designed to assess the kinetic component of RHL perturbation of the metal center's small-molecule binding properties upon ligand-based oxidation. These experiments show that acetonitrile is kinetically labile with respect to Ru(II) in **4a**$^+$, but not **4a**, on the time scale of the NMR experiment. Significantly, acetonitrile is the only one of the substrates examined by $^2H\{^1H\}$ NMR studies with **4a**$^+$ which reacts with **4a** in a 1:1 ratio of **4a** to substrate in methylene chloride under ambient conditions. In contrast, ethylene, thiophene, and acetone need more extreme conditions to force the reaction with **4a** to occur, such as elevated temperature, coordinating solvents, or high concentration of target substrates. This demonstrates that, although the binding constant changes of the metal center for small molecules is expected to increase by 3 orders of magnitude upon ligand-based oxidation of **4a** to **4a**$^+$, this change will not always translate into an observable change in the lability of the small molecule with respect to the metal center. Thus, in the design of RHL−metal complexes for molecular uptake and release, the target substrate should be selected and the complex specifically designed to (1) maximize the RHL effect and (2) ensure that the oxidation-induced changes in the metal−RHL binding interaction yield changes in the binding properties of the metal center for the small molecule of interest.

Conclusions

Polymerizable, terthienyl-based RHLs, their corresponding Ru(II) complexes, and polymers formed from these complexes have been designed, synthesized, and characterized. These complexes provide a model for understanding the factors that affect hole delocalization within metal-bound oligothienyl units. Moreover, the systematic study reported herein provides an important lesson regarding the design of tunable ligands that can be used to electrochemically modulate bound metal center properties. Specifically, efforts directed at preparing conducting polymer−metal hybrid materials for tunable redox control over bound transition metal properties must balance (1) the need for metal centers with high oxidation potentials and (2) the observation that cationic repulsion between the bound metal centers and the oxidized conducting polymer can effectively localize holes within the conducting polymer backbone and limit the tunability of metalated conducting polymer materials. Notably, the results suggest that if one wants a truly delocalized system where the incremental removal of charge from the conducting polymer results in an incremental change in the electronic properties of the bound metal centers, one should reduce the ratio of metal centers to oligothienyl repeat units within the polymeric structure.

Experimental Section

General. All reactions were carried out under a dry nitrogen atmosphere using standard Schlenk techniques or in an inert-atmosphere glovebox unless otherwise noted. Acetonitrile, dichloromethane, and pentane were dried over calcium hydride. Tetrahydrofuran (THF) and diethyl ether were dried over sodium/benzophenone. Acetone (HPLC grade) was purchased from Acros Organics and used as received. All solvents were distilled under nitrogen and saturated with N_2 prior to use. Deuterated solvents and ethylene-d_4 were purchased from Cambridge Isotope Laboratories and used without further purification. $LiB(C_6F_5)_4 \cdot Et_2O$ was purchased from Boulder Scientific and used as received. Silver(I) tetrafluoroborate, *tert*-butylisonitrile, carbon monoxide, and ethylene were purchased from Aldrich Chemical Co. and used as received. Thiophene and *n*-Bu_4NPF_6 were purchased from Aldrich Chemical Co. and purified as previously reported[61] and by recrystallization three times from hot ethanol followed by heating in vacuo for 3 days, respectively. Precious metals were purchased from D. F. Goldsmith, Evanston, IL. A gold minigrid was purchased from Buckbee Mears, St. Paul, MN.

Physical Measurements. ^1H, $^{31}P\{^1H\}$, $^{19}F\{^1H\}$, and $^{13}C\{^1H\}$ NMR spectra were recorded on a Varian Gemini 300-MHz FT-NMR spectrometer, a Varian Unity 400-MHz FT-NMR spectrometer, or a Varian Mercury 300-MHz FT-NMR. $^{31}P\{^1H\}$ NMR spectra were externally referenced relative to 85% H_3PO_4, $^{19}F\{^1H\}$ NMR spectra were externally referenced relative to $CFCl_3$, and ^1H NMR spectra were referenced relative to residual solvent peaks. To achieve accurate integrations for cyclopentadiene-containing complexes, a 40-s pulse delay between scans was used to allow all protons to relax. Variable-temperature ^1H and $^{31}P\{^1H\}$ NMR spectra were recorded on a Varian Unity 400-MHz FT-NMR at 400 and 162 MHz, respectively, or a Varian Mercury 300-MHz FT-NMR at 300 and 121 MHz, respectively.

(61) Spies, G. H.; Angelici, R. J. *Organometallics* **1987**, *6*, 1897−1903.

Variable-temperature $^2H\{^1H\}$ NMR spectra were recorded on a Varian Unity 400-MHz FT-NMR at 61 MHz. FT-IR spectra were recorded using a Nicolet 520 FT-IR spectrometer. UV−vis spectra were recorded using an HP 8452A or HP 845x spectrometer. Electrochemical measurements were carried out on either a PINE AFRDE4 or an AFRDE5 bipotentiostat/galvanostat using Au, Pt, or glassy carbon disk electrodes with a Pt mesh counter electrode and a $Ag/AgNO_3$ (0.01 M $AgNO_3$ in CH_3CN/0.1 M *n*-Bu_4NPF_6; BAS, West Lafayette, IN) reference electrode, a Ag/AgCl reference electrode (Cypress Systems, Lawrence, KS), or a silver wire quasi-reference electrode. All electrochemical data were referenced versus an internal $FcH/[FcH]^+$ ($Fc = (\eta^5\text{-}C_5H_5)Fe(\eta^5\text{-}C_5H_4)$) redox couple unless noted otherwise. Spectroelectrochemistry (FT-IR) was performed in a cell consisting of NaCl plates sandwiched together with a Teflon spacer.[14] The electrodes placed in the internal volume of the cell were a Pt mesh or Pt wire counter electrode, a Ag wire or Ag/AgCl reference electrode, and a Au minigrid working electrode for transmittance in situ monitoring of the oxidation products. Electron impact (EI) and fast atom bombardment (FAB) mass spectra were recorded using a Fisions VG 70-250 SE mass spectrometer. Electrospray (ES) mass spectra were recorded using a Micromass Quatro II electrospray triple-quadrapole mass spectrometer. EPR spectra were measured using a modified Varian E-4 X-band spectrometer, and the field was calibrated using diphenylpicrylhydrazyl (dpph) as a standard. Elemental analyses were performed by Desert Analytics Laboratory, Tuscon, AZ. Energy dispersive spectroscopy (EDS) was performed on a Hitachi scanning electron microscope equipped with an EDS detector. Compounds **1a**−**5a** and **1b**−**4b** were prepared as previously reported.[14]

[CpRuCO(κ^2-3′-(2-diphenylphosphinoethyl)-5,5″-dimethyl-2,2′:5′,2″-terthiophene)][B(C_6F_5)$_4$]$_2$ (4a$^+$). In a typical experiment, 10−20 mg of **4a** was dissolved in 6 mL of CH_2Cl_2 with 50 mg of $LiB(C_6F_5)_4\cdot Et_2O$ (0.07 mmol) as electrolyte and added to one side of a two-compartment cell which held a working electrode (Pt mesh) and a reference electrode (Ag/AgCl). Separated from the complex solution by a frit was 50 mg of $LiB(C_6F_5)_4\cdot Et_2O$ dissolved in 6 mL of CH_2Cl_2 and the counter electrode (Pt mesh). Electrochemical oxidation to a potential beyond the first oxidation potential of the complex with stirring overnight yielded the blue **4a**$^+$ from green **4a**. Conversion was complete as monitored by UV−vis spectroscopy. ^1H NMR (CD_2Cl_2): featureless. $^{31}P\{^1H\}$ NMR (CD_2Cl_2): featureless. $^{19}F\{^1H\}$ NMR (CD_2Cl_2): δ −133.2 (s), −163.4 (s), −167.4 (s). IR (CH_2Cl_2): ν_{CO} ∼2006 cm^{-1} (this frequency is a lower limit to the accurate value due to overlap of the band with the band of any residual **4a**). UV−vis λ_{max} (CH_2Cl_2): 656 (br) nm. X-band EPR (CH_2Cl_2, 298K): $g = 2.003$, width = 30 G.

[Cp(CH$_3$CN)RuCO(3′-(2-diphenylphosphinoethyl)-5,5″-dimethyl-2,2′:5′,2″-terthiophene)][B(C_6F_5)$_4$]$_2$ (5a$^+$). Complex **5a** (6 mg, 4 × 10^{-3} mmol) was electrochemically oxidized in a manner similar to the formation of **4a**$^+$ with 50 mg of $LiB(C_6F_5)_4\cdot Et_2O$ (0.05 mmol) in 6 mL of CH_2Cl_2 on each side of the electrochemical cell. Oxidation overnight yielded a deep blue-colored solution comprised of a mixture of the target complex and electrolyte. Removal of solvent yielded a solid mixture of **5a**$^+$ and electrolyte. UV−vis λ_{max} (CH_2Cl_2): 685 nm (br). X-band EPR (CH_2Cl_2, 298K): $g = 2.0025 \pm 0.0005$, width = 30 G.

Acetonitrile Adduct of 4b: [Cp(CH$_3$CN)RuCO(3′-(2-diphenylphosphinoethyl)-2,2′:5′,2″-terthiophene)][B(C_6F_5)$_4$] (5b). This complex was prepared by dissolving **4b** (15 mg, 9.7 × 10^{-3} mmol) in 0.5 mL of CH_3CN for 24 h under ambient conditions. Over the course of the reaction, the orange solution became pale yellow. The CH_3CN was removed in vacuo and the product characterized. The CH_3CN can be quantitatively removed to re-form **4b** by heating the sample to 100 °C in vacuo for 5 d. ^1H NMR (CD_2Cl_2): δ 7.58−7.37 (m, 10H, Ph); 7.36 (dd, 1H, $J_{3-5} = 1.0$, $J_{5-4} = 5.3$, 5″ or 5 thienyl); 7.29 (dd, 1H, $J_{3-5} = 1.0$, $J_{5-4} = 5.3$, 5″ or 5 thienyl); 7.20 (dd, 1H, $J_{3-5} = 1.2$, $J_{3-4} = 3.6$, 3 or 3″ thienyl); 7.06 (2 overlapping dd, 2H, 4 and 4″ thienyl); 6.98 (overlapping dd and s, 2H, 4′ thienyl and 3 or 3″); 5.03 (s, 5H, Cp); 2.78 (s (br), 4H, CH_2CH_2); 2.09 (s, 3H, CH_3CN). $^{31}P\{^1H\}$ NMR (CD_2Cl_2): δ (s) 42.1. IR (CH_2Cl_2): $\nu_{CO} = 1994$ cm^{-1}. MS (ES) [M^+]: calcd for $C_{34}H_{29}NOPRuS_3$, *m*/*z* 696; found, *m*/*z* 696. UV−vis λ_{max} (CH_2Cl_2): = 341 nm.

Poly-4b. In a typical preparation, **4b** (30 mg, 0.02 mmol), 70 mg of $LiB(C_6F_5)_4\cdot Et_2O$ (0.10 mmol), and 3 mL of CH_2Cl_2 are added to a well-shaped electrochemical cell.[62] A rectangle of Au foil forms the bottom of the electrochemical cell, and the working, reference (Ag wire), and counter (Pt mesh) electrodes are held in solution above the working electrode. Cycling the potential between 0 and 900 mV vs Ag wire for 48 h at 50 mV/s yields the surface-immobilized polymer and a mixture of oligomers. Reduction of any oxidized species at −200 mV for several hours yields the orange polymer and oligomers in the neutral oxidation state.

3′,4‴′-Bis{CpRuCOCl(2-diphenylphosphinoethyl)}-2,2′:5′,2″:5″,2‴:5‴,2⁗:5⁗, 2⁗′-sexithiophene (6). The solvent is removed from the resulting solution after a typical preparation of poly-**4b** and the solutions from several polymer preparations are combined. Typically, a mixture of oligomers corresponding to 125 mg of monomer (0.09 mmol) is combined in 5 mL of acetone under ambient conditions, 100 mg (1.3 mmol) of KCl is added, and the mixture is refluxed for 3 d. Removal of solvent and column chromatography on alumina using methylene chloride as eluent followed by preparative TLC (alumina/methylene chloride) allows for the isolation of a bright yellow band. Recrystallization from CH_2Cl_2 (3 mL)/ pentane (20 mL) yields the desired product in 66% yield as orange-yellow blocks. ^1H NMR (CD_2Cl_2): δ 7.61−7.41 (m, 20 H); 7.28 (dd, 2 H, $J = 0.6$, 3.0); 7.10−7.07 (m, 6 H); 7.01−6.97 (m, 4 H); 4.83 (s, 10 H, Cp); 3.21−3.13 (m, 2 H, CH_2); 2.99−2.91 (m, 2 H, CH_2); 2.71−2.58 (m, 4 H, CH_2). $^{31}P\{^1H\}$ NMR (CD_2Cl_2): δ 45.2 (s). $^{13}C\{^1H\}$ NMR (CD_2Cl_2): δ 205.5 (d, $J_{C-P} = 15.1$, CO); 139.8 (s); 139.6 (s); 138.6 (s); 138.0 (s); 136.3 (s); 136.2 (s); 135.5 (s); 135.3 (s); 134.3 (s); 134.2 (s); 133.9 (s); 133.3 (s); 131.7 (s); 131.5 (s); 131.4 (s); 130.4 (s); 129.2 (s); 129.0 (s); 128.9 (s); 128.8 (s); 128.1 (s); 126.8 (s); 126.8 (s); 126.1 (s); 124.9 (s); 86.3 (s, Cp); 30.1 (d, $J_{C-P} = 30.2$, *C*H_2CH$_2$P); 24.4 (s, CH$_2$*C*H$_2$P) (phenyl and thienyl resonances not assigned). IR (CH_2Cl_2): $\nu_{CO} = 1955$ cm^{-1}. MS (FAB$^+$) [M^+]: calcd for $C_{64}H_{50}Cl_2O_2P_2Ru_2S_6$, *m*/*z* 1377.9; found, *m*/*z* 1378.6. UV−vis λ_{max} (CH_2Cl_2): 430 nm.

[3′,4‴′-Bis{CpRuCO(κ^2-(2-diphenylphosphinoethyl))}-2,2′:5′,2″:5″,2‴:5‴,2⁗:5⁗,2⁗′-sexithiophene][B(C_6F_5)$_4$]$_2$ (7). Complex **6** (43 mg, 0.03 mmol) was dissolved in 5 mL of CH_2Cl_2 with $LiB(C_6F_5)_4\cdot Et_2O$ (35 mg, 0.046 mmol) and stirred under N_2 for 7 d to abstract the chloride anion. Filtration to remove LiCl, removal of solvent in vacuo, and recrystallization from CH_2Cl_2 (5 mL)/ pentane (20 mL) yields **7** as a pure, air-stable, orange-red powder which has limited solubility in CH_2Cl_2. ^1H NMR (CD_2Cl_2): δ 7.44−7.26 (m, 26 H); 7.12 (d, 2 H, $J = 4$); 6.98 (d, 2 H, $J = 4$); 6.63 (s, 2 H); 4.90 (s, 10 H, Cp); 3.20−3.05 (m, 8 H, CH_2CH_2). $^{31}P\{^1H\}$ NMR (CD_2Cl_2): δ 39.9 (s). $^{19}F\{^1H\}$ NMR (CD_2Cl_2): δ −133.6 (s); −164.0 (t, $J = 20.2$); −167.9 (s). IR (CH_2Cl_2): ν_{CO} = 1996 cm^{-1}. MS (ES) [M^+]: calcd for [$C_{64}H_{50}S_6Ru_2P_2O_2$][$BC_{24}F_{20}$], *m*/*z* 1986.9; found, *m*/*z* 1986.3. UV−vis λ_{max} (CH_2Cl_2): 456 nm.

[3′,4‴′-Bis{CpRuCO(κ^2-(2-diphenylphosphinoethyl))}-2,2′:5′,2″:5″,2‴:5‴,2⁗:5⁗,2⁗′-sexithiophene][B(C_6F_5)$_4$]$_3$ (7$^+$). Complex **7** was oxidized using the same apparatus as for oxidation of **4a**, using 7 (3 mg, 1 × 10^{-3} mmol) with 6 mL of CH_2Cl_2 and 50 mg of $LiB(C_6F_5)_4\cdot Et_2O$ (0.07 mmol) on each side of the electrochemical cell. Overnight oxidation yielded a color change from red to green. The solvent was removed to yield a green solid which is a mixture of **7**$^+$ and electrolyte. UV−vis λ_{max} (CH_2Cl_2): 762 nm. EPR (CH_2Cl_2, 298 K): $g = 2.002$.

[3′,4‴′-Bis{Cp(CH$_3$CN)RuCO(2-diphenylphosphinoethyl)}-2,2′:5′,2″:5″,2‴:5‴,2⁗:5⁗,2⁗′-sexithiophene][B(C_6F_5)$_4$]$_2$ (8). Complex 7 (6 mg, 2 × 10^{-3} mmol) is dissolved in 1 mL of CH_3CN and shaken at room temperature under ambient conditions for 4 d with a change from a red-orange sparingly soluble complex to a bright yellow, freely soluble complex. Removal of CH_3CN and addition of CD_2Cl_2 allows for monitoring the ^1H NMR spectroscopy which shows a 100% spectroscopic yield. ^1H NMR (CD_2Cl_2): δ 7.58−7.32 (m, 22 H); 7.09−6.94 (m, 10 H); 5.02 (s, 10 H, Cp); 2.78 (m, 8 H, CH_2CH_2); 2.07 (s, 6 H, coordinated CH_3CN). $^{31}P\{^1H\}$ NMR (CD_2Cl_2): δ 41.7 (s). $^{19}F\{^1H\}$ NMR (CD_2Cl_2): δ −133.4 (s); −163.9 (t, $J = 19.9$); −167.8 (s). IR (CH_2Cl_2): $\nu_{CO} = 1993$ cm^{-1}. MS (ES) [M^+]: calcd for [$C_{68}H_{56}N_2O_2P_2Ru_2S_6$][$BC_{24}F_{20}$], *m*/*z* 2069.0; found, *m*/*z* 2069.2. UV−vis λ_{max} (CH_2Cl_2): 430 nm.

(62) Sailor, M. J., Heinrich, J. L., Lauerhaas, J. M., Kamat, P. V., and Meisel, D., Eds.; Elsevier Science: New York, 1997; Vol. 103, pp 209−235.

[3′, 4‴′-Bis{Cp(CH$_3$CN)RuCO(2-diphenylphosphinoethyl)}-2,2′:5′,2″:5″,2‴:5‴,2⁗:5⁗,2⁗′-sexithiophene][B(C$_6$F$_5$)$_4$]$_3$ (8$^+$). Electrochemical oxidation of **8** (6 mg, 2.2×10^{-3} mmol) in a manner similar to that described for **4a** with 50 mg of LiB(C$_6$F$_5$)$_4$·Et$_2$O and 6 mL of CH_2Cl_2 on each side of the electrochemical cell yielded a green-colored solution of **8**$^+$ and electrolyte. Removal of solvent yielded a green-brown-colored solid mixture of **8**$^+$ and electrolyte. UV−vis λ_{max} (CH_2Cl_2): 763 nm. EPR (CH_2Cl_2, 298 K): $g = 2.0025 \pm 0.0005$.

***tert*-Butylisonitrile Adduct of 4a: [Cp((CH$_3$)$_3$CNC)RuCO(3′-(2-diphenylphosphinoethyl)-5,5″-dimethyl-2,2′:5′,2″-terthiophene)][B(C$_6$H$_3$-3,5-(CF$_3$)$_2$)$_4$] (9).** This complex was prepared in quantitative spectroscopic yield by mixing **4a** (15 mg, 9.7×10^{-3} mmol) and 5 equiv of $(CH_3)_3CNC$ (5.5 μL) in 0.7 mL of CD_2Cl_2 at room temperature for 12 d. Heating the sample to 100 °C in vacuo (<50 mTorr) for 5 d does not result in the re-formation of **4a**. ^{1}H NMR (CD_2Cl_2): δ 7.71 (br, 8 H, Ar′); 7.56 (br, 4 H, Ar′); 7.54−7.38 (m, 10 H, Ph); 6.96 (d, $J_{3-4} = 3.3$, 1 H, 3 or 3″ thienyl); 6.83 (s, 1 H, 4′ thienyl); 6.72 (d, $J_{3-4} = 3.3$, 1 H, 3 or 3″ thienyl); 6.68 (2 overlapping dd, 2 H, 4 and 4″ thienyl); 5.12 (s, 5H, Cp); 2.76−2.70 (m, 4 H, CH_2CH_2); 2.48 (d, $J_{Me-4} = 1.2$, 3 H, CH_3); 2.45 (d, $J_{Me-4} = 1.2$, 3 H, CH_3); 1.29 (s, 9H, CNC(CH_3)$_3$). ^{31}P{^{1}H} NMR (CD_2Cl_2): δ 42.7 (s). IR (CH_2Cl_2): $\nu_{CO} = 2003$ cm^{-1}, $\nu_{CN} = 2176$ cm^{-1}. UV−vis λ_{max} (CH_2Cl_2): 354 nm. MS (ES) [M^+]: calcd for $C_{39}H_{39}NOPRuS_3$, *m*/*z* 766; found, *m*/*z* 766.0.

Acetone-d_6 Adduct of 4a: [Cp(CD$_3$C(O)CD$_3$)RuCO(3′-(2-diphenylphosphinoethyl)-5,5″-dimethyl-2,2′:5′,2″-terthiophene)][B(C$_6$H$_3$-3,5-(CF$_3$)$_2$)$_4$] (10). This adduct can be generated by the addition of 0.7 mL of acetone-d_6 to 60 mg of **4a**. ^{1}H and ^{31}P{^{1}H} NMR spectroscopies indicate approximately 9% conversion to the acetone adduct. Due to the low concentration of **10** relative to that of **4a**, the full ^{1}H NMR spectrum cannot be reported. However, the ^{1}H NMR Cp (δ 5.33) and ^{31}P{^{1}H} NMR resonances (δ 46.3) are distinguishable from those of **4a** in acetone (δ 5.27 and 41.5, respectively). The assignment of **4a** and **10** in acetone was made by examining the variable-temperature ^{31}P{^{1}H} NMR spectra (see Supporting Information). The resonance assigned to **4a** at room temperature splits into two separate resonances (δ 53.3 and 35.1) at −80 °C due to pyramidal inversion of the bound S atom, which yields diastereomers with different chemical shifts. In contrast, the resonance assigned to **10** remains sharp and of constant intensity from room temperature to −80 °C. Removal of acetone-d_6 in vacuo quantitatively removes the bound acetone to re-form **4a**. It should be noted that the addition of acetone (100 equiv) to a CD_2Cl_2 solution of **4a** does not result in the formation of **10**. Confirmation of adduct formation was obtained by mass spectrometry of **4a** in acetone. However, the mode of acetone coordination has not been determined. MS (ES) [M^+]: calcd for $C_{38}H_{36}O_2PRuS_3$, *m*/*z* 741; found, *m*/*z* 741.

CO Adduct of 4a: [Cp(CO)RuCO(3′-(2-diphenylphosphinoethyl)-5,5″-dimethyl-2,2′:5′,2″-terthiophene)][B(C$_6$H$_3$-3,5-(CF$_3$)$_2$)$_4$] (11). The addition of CO to an NMR tube containing 15 mg (9.7×10^{-3} mmol) of **4a** in 0.7 mL of CD_2Cl_2 at room temperature or at 50 °C for 3 d yielded no product. Removal of the solvent, addition of acetone-d_6 (0.6 mL), recharging the tube with CO, and shaking at room temperature for 3 d yielded about 9% product conversion. Heating the sample to 50 °C for 13 d yielded the desired product in 94% spectroscopic yield. ^{1}H NMR (CD_2Cl_2): δ 7.73 (br, 8 H, Ar′); 7.56 (br, 4 H, Ar′); 7.49−7.40 (m, 10 H, Ph); 6.96 (d, $J_{3-4} = 3.6$, 1 H, 3 or 3″ thienyl); 6.81 (s, 1 H, 4′ thienyl); 6.73 (d, $J_{3-4} = 3.6$, 1 H, 3 or 3″ thienyl); 6.69 (2 overlapping dd, 2 H, 4 and 4″ thienyl); 5.36 (s, 5 H, Cp); 2.83−2.73 (m, 4 H, CH_2CH_2); 2.47 (d, $J_{Me-4} = 0.6$, 3 H, CH_3); 2.46 (d, $J_{Me-4} = 1.2$, 3 H, CH_3). ^{31}P{^{1}H} NMR (CD_2Cl_2): δ 38.9 (s). IR (CH_2Cl_2): $\nu_{CO} = 2021$, 2066 cm^{-1}. UV−vis λ_{max} (CH_2Cl_2): 348 nm. MS (ES) [M^+]: calcd for $C_{35}H_{30}O_2PRuS_3$, *m*/*z* 711.0; found *m*/*z* 711.0.

Ethylene Adduct of 4a: [Cp(C$_2$H$_4$)RuCO(3′-(2-diphenylphosphinoethyl)-5,5″-dimethyl-2,2′:5′,2″-terthiophene)][B(C$_6$H$_3$-3,5-(CF$_3$)$_2$)$_4$] (12). The addition of ethylene to an NMR tube containing 15 mg (9.7×10^{-3} mmol) of **4a** in 0.7 mL of CD_2Cl_2 at room temperature for 3 d yielded a minor amount of product. Heating the sample to 50 °C for 22 d results in a final spectroscopic yield of 93%. ^{1}H NMR (CD_2Cl_2): δ 7.73 (br, 8 H, Ar′); 7.56 (br, 4 H, Ar′); 7.50−7.20 (m, 10 H, Ph); 6.96 (d, $J_{3-4} = 3.3$, 1 H, 3 or 3″ thienyl); 6.81 (s, 1 H, 4′ thienyl); 6.74 (d, $J_{3-4} = 3.5$, 1 H, 3 or 3″ thienyl); 6.71 (dd, $J_{4-Me} = 0.9$, $J_{3-4} = 3.6$, 1 H, 4 or 4″ thienyl); 6.69 (dd, $J_{4-Me} = 0.9$, $J_{3-4} = 3.6$, 1 H, 4 or 4″ thienyl); 5.21 (s, 5H, Cp); 3.15−3.08 (m, 4H, bound ethylene); 2.65 (s (br), 4 H, CH_2CH_2); 2.47 (s, 6 H, CH_3). ^{31}P{^{1}H} NMR (CD_2Cl_2): δ 43.1 (s). IR (CH_2Cl_2): $\nu_{CO} = 2010$ cm^{-1}; UV−vis λ_{max} (CH_2Cl_2): 348 nm. MS (ES) [M^+]: calcd for $C_{36}H_{34}OPRuS_3$, *m*/*z* 711.1; found, *m*/*z* 711.0.

Thiophene Adduct of 4a: [Cp(C$_4$H$_4$S)RuCO(3′-(2-diphenylphosphinoethyl)-5,5″-dimethyl-2,2′:5′,2″-terthiophene)][B(C$_6$H$_3$-3,5-(CF$_3$)$_2$)$_4$] (13). The addition of 1 equiv of thiophene (0.78 μL) to an NMR tube containing 15 mg (9.7×10^{-3} mmol) of **4a** in 0.7 mL of CD_2Cl_2 did not yield any thiophene adduct after 3 d at room temperature or with mild heating. The CD_2Cl_2 was removed, and acetone-d_6 was added. Similarly, no reaction occurred after 3 d at room temperature or with mild heating. Dissolving **4a** in neat thiophene (10 mL) at room temperature for 1 d leads to formation of a thiophene adduct. Removal of excess thiophene in vacuo and dissolution of the resulting product in CD_2Cl_2 allows for characterization of the resulting thiophene adduct, formed in 1:1.1 ratio to **4a**. ^{1}H NMR (CD_2Cl_2): δ 4.75 (s, Cp). ^{31}P{^{1}H} NMR (CD_2Cl_2): δ 39.4. MS (ES) [M^+]: calcd for $C_{38}H_{34}OPRuS_4$, *m*/*z* 767; found, *m*/*z* 767.

Acknowledgment. We acknowledge the NSF (CHE-0071885) for generously funding this research.

Supporting Information Available: Tables of crystal data, structure solution and refinement, atomic coordinates, bond lengths and angles, and anisotropic thermal parameters for **2a, 4a, 4b,** and **6**; spectroscopic data for **1a**−**5a**, **1b**−**4b**; EPR spectra for **4a**$^+$, **5a**$^+$, **7**$^+$, and **8**$^+$ (PDF). This material is available free of charge via the Internet at http://pubs.acs.org.

JA0030008